AMERICAN SOCIETY FOR MICROBIOLOGY | Molecular and Cellular Biology®

RESEARCH ARTICLE

OtDUB from the Human Pathogen *Orientia tsutsugamushi* Modulates Host Membrane Trafficking by Multiple Mechanisms

Jason M. Berk,[a]* Min Jae Lee,[a] Mengwen Zhang,[a,b] Christopher Lim,[a] Mark Hochstrasser[a,c]

[a]Department of Molecular Biophysics and Biochemistry, Yale University, New Haven, Connecticut, USA
[b]Department of Chemistry, Yale University, New Haven, Connecticut, USA
[c]Department of Molecular, Cellular and Developmental Biology, Yale University, New Haven, Connecticut, USA

ABSTRACT Host cell membrane-trafficking pathways are often manipulated by bacterial pathogens to gain cell entry, avoid immune responses, or to obtain nutrients. The 1,369-residue OtDUB protein from the obligate intracellular human pathogen *Orientia tsutsugamushi* bears a deubiquitylase (DUB) and additional domains. Here we show that OtDUB ectopic expression disrupts membrane trafficking through multiple mechanisms. OtDUB binds directly to the clathrin adaptor-protein (AP) complexes AP-1 and AP-2, and the $OtDUB_{275–675}$ fragment is sufficient for binding to either complex. To assess the impact of OtDUB interactions with AP-1 and AP-2, we examined *trans*-Golgi trafficking and endocytosis, respectively. Endocytosis is reduced by two separate OtDUB fragments: one contains the AP-binding domain ($OtDUB_{1–675}$), and the other does not ($OtDUB_{675–1369}$). $OtDUB_{1–675}$ disruption of endocytosis requires its ubiquitin-binding capabilities. $OtDUB_{675–1369}$ also fragments *trans*- and *cis*-Golgi structures. Using a growth-based selection in yeast, we identified viable $OtDUB_{675–1369}$ point mutants that also no longer caused Golgi defects in human cells. In parallel, we found $OtDUB_{675–1369}$ binds directly to phosphatidylserine, and this lipid binding is lost in the same mutants. Together these results show that OtDUB contains multiple activities capable of modulating membrane trafficking. We discuss how these activities may contribute to *Orientia* infections.

KEYWORDS *Orientia*, clathrin adaptor proteins, endocytosis, Golgi, membrane trafficking, phosphatidylserine, ubiquitin, scrub typhus

Scrub typhus is a neglected tropical disease endemic to Southeast Asia (1). The disease has a wide spectrum of symptoms, making diagnosis difficult, and is often mistaken for other febrile diseases, such as dengue fever. Over one million people a year are diagnosed with scrub typhus and the median mortality rate is 6% and 1.4% for untreated and antibiotic treated patients, respectively (2). The causative agent is the obligate intracellular Gram-negative bacterium *Orientia tsutsugamushi*. Transmission to humans, which are dead-end hosts, occurs when one is bitten by infected larval mites (commonly called chiggers) from the *Leptotrombidium* genus (2). The bacterium exhibits tropism for dendritic cells, monocytes, macrophages, and endothelial cells (3) and also invades nonphagocytic cells through clathrin-mediated endocytosis (4). Through unknown means, the bacteria escape to the cytosol from the phagosomal or endosomal vesicles; they replicate in a polysaccharide-enriched niche near the microtubule organizing center. While *O. tsutsugamushi* effects on host cell-signaling pathways have been well characterized (3), analyses of bacterial proteins that allow for host occupancy are also now gaining traction (5–11).

One such protein, OtDUB, was originally identified by computational screening for ubiquitin-like protein (Ubl)-specific protease (Ulp1-like or C48 family) domains (12–14). The presence of a ubiquitin pathway enzyme in the genome of a bacterial pathogen suggests the protein is important for infection as the ubiquitin-proteasome system (UPS) plays numerous roles in host cell defense and bacteria lack their own UPS. Biochemical analysis of the

Address correspondence to Mark Hochstrasser, mark.hochstrasser@yale.edu.

*Present address: Jason M. Berk, Arvinas, Inc., New Haven, Connecticut, USA.

The authors declare no conflict of interest.

Received 4 March 2022
Returned for modification 19 March 2022
Accepted 26 May 2022
Published 21 June 2022

Ulp1-like domain revealed a ubiquitin-specific deubiquitylase (DUB) with activity toward various ubiquitin chain linkage types and a preference for cleaving longer chains (12).

Just downstream of the N-terminal DUB domain is a high-affinity ubiquitin-binding domain (UBD) that regulates the DUB domain and modulates its specificity (12). When expressed in yeast, OtDUB causes a complete inhibition of growth, but this effect is DUB/UBD independent (15). A proteomics screen identified multiple host proteins that could interact with the fragment causing yeast toxicity. Two of those interactors were the Rho GTPases CDC42 and Rac1, which led to the discovery and characterization of a cryptic Rac1 guanine nucleotide exchange factor (GEF) domain in OtDUB. The GEF activity, however, was also not responsible for the yeast toxicity (15).

Mass spectrometry identified additional human proteins that bind OtDUB, including multiple subunits of the clathrin adaptor protein (AP) complexes AP-1 and AP-2 (15). AP complexes are heterotetramers involved in intracellular vesicle trafficking (16). These complexes recognize the sorting signals in the cytoplasmic tails of membrane-embedded cargo proteins, thereby recruiting the coat protein clathrin and accessory factors. These proteins in turn drive membrane invagination and formation of vesicles that transport the cargo to target membranes. AP-1 is responsible for the forward and retrograde trafficking of proteins between the *trans*-Golgi network (TGN) and endosomes and lysosomes, while AP-2 is required for clathrin-mediated endocytosis from the plasma membrane (16).

Given the plethora of ways membrane trafficking is exploited by bacterial pathogens, the interactions with AP-1 and AP-2 were further pursued here. We first verified that OtDUB binds directly to AP-1 and AP-2 and then identified a region of OtDUB sufficient for binding AP-1/2 ($OtDUB_{275–675}$). Ectopic expression of full-length OtDUB in HeLa cells disrupted both AP-1-dependent TGN trafficking and AP-2-dependent endocytosis. Endocytosis was disrupted by two different OtDUB fragments, one ($OtDUB_{1–675}$) containing the AP-1/2 binding domain (AP-1/2BD) and the other ($OtDUB_{675–1369}$) not. TGN trafficking was only disrupted by OtDUB in an AP-1/2BD-independent manner (by $OtDUB_{675–1369}$), and expression of this domain fragmented Golgi stacks. This Golgi-dispersing domain overlapped with a minimal domain ($OtDUB_{650–1159}$) required for toxicity in yeast.

Utilizing a growth-based yeast assay, we identified a panel of single-residue mutations in OtDUB that suppressed its toxicity in yeast; these mutations in $OtDUB_{675–1369}$ also prevented membrane trafficking defects in HeLa cells. In parallel, $OtDUB_{675–1369}$ was found to bind directly to phosphatidylserine (PS); the tested suppressor mutants no longer bound to PS, suggesting the trafficking defects induced by $OtDUB_{675–1369}$ occurred through interaction with and/or modification of the PS phospholipid. Cumulatively, our data reveal that OtDUB has several mechanisms by which it interacts with and modulates host membrane-trafficking pathways; these are predicted to play important roles in bacterial infection.

RESULTS

OtDUB binds AP-1 and AP-2 directly *in vitro* and in cells. Peptides from multiple subunits of the clathrin adaptor protein complexes 1 and 2 were greatly enriched in a previously reported proteomics screen for OtDUB interactors (15). To validate these hits and to examine AP-1/2 association in the context of the known binding of ubiquitin to OtDUB (12), we performed binding assays using HeLa cell lysates and the recombinant, mutationally inactivated DUB $OtDUB_{C135A}$-Flag. To maintain ubiquitin-conjugate levels, cells were lysed in the presence of *N*-ethylmaleimide (NEM) to inhibit host DUB proteases by alkylation of their active-site cysteines. OtDUB readily bound both free ubiquitin (Ub_1) and (poly)ubiquitin conjugates (Ub_n) with more conjugates present in the NEM-treated lysates (Fig. 1A). Representative subunits of both AP-1 and AP-2 were strongly enriched in the OtDUB pulldowns, confirming the original proteomics results. Unexpectedly, the interactions with AP-1/2 were almost eliminated by NEM treatment (Fig. 1A, right lane) (discussed further below).

To determine if OtDUB binds AP-1 and AP-2 complexes directly, purified recombinant $OtDUB_{C135A}$ was incubated with recombinant core complexes of AP-1 and AP-2 and then resolved in a gel-filtration peak-shift assay. When the AP-2 core alone was passed through the column, a single peak eluted at ~15.7 mL. OtDUB alone eluted at ~12.6 mL and the

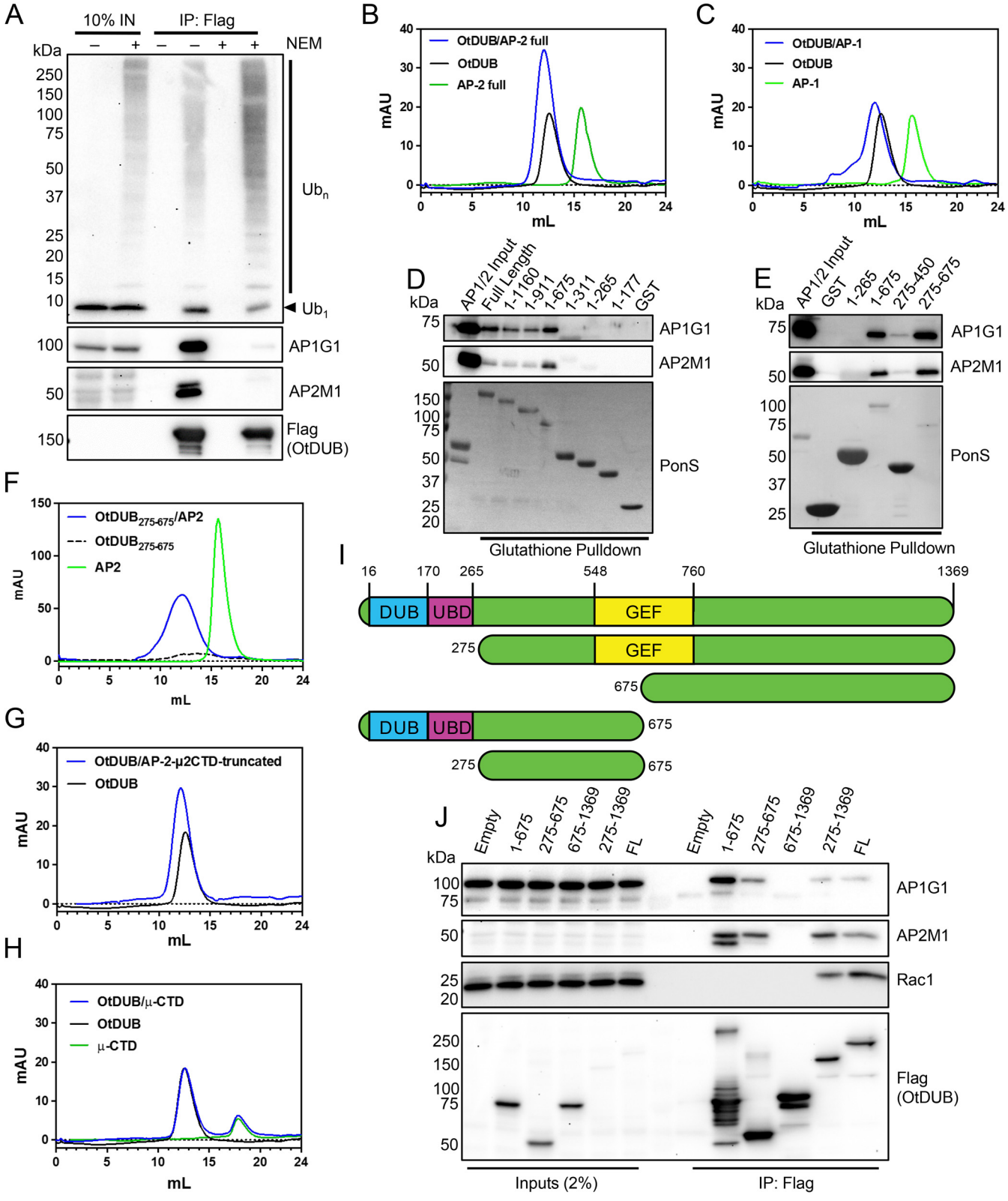

FIG 1 OtDUB associates directly with adapter protein-1 and -2 (AP-1 and AP-2). (A) HeLa cell lysates treated with 30 mM *N*-ethylmaleimide (NEM) (+/−) were incubated with anti-Flag-resin or immobilized OtDUB-Flag resin. Input lysates and eluates were tested for putative binding partners by SDS-PAGE and immunoblotting (n = 1). Arrowhead denotes monoubiquitin (Ub$_1$), Ub$_N$, ubiquitin conjugates. Numbers on the left in this panel and elsewhere indicate molecular mass markers (in kDa). (B and C) Superose 6 gel filtration chromatograms of purified proteins: AP2 core alone (green), OtDUB alone (black), or the complex of both (blue) (n = 2) (B); AP1 core alone (green), OtDUB alone (black), or the complex of both (blue) (n = 1) (C). (D) C-terminal truncations of

(Continued on next page)

complex of the two proteins resolved earliest as a single, enlarged peak at ~12.1 mL, indicating direct interaction (Fig. 1B). Comparable results were seen with AP-1 (Fig. 1C).

A truncation analysis was carried out to determine the region of OtDUB sufficient for binding the adaptor protein complexes directly (Fig. 1D and E). In this assay, bacterial lysates containing recombinantly expressed GST-tagged OtDUB fragments were incubated with purified recombinant AP-1 and AP-2 core complexes followed by glutathione-resin enrichment and isolation. When C-terminal truncations were examined, $OtDUB_{1–675}$ was the shortest fragment still capable of binding AP-1 and AP-2 (Fig. 1D). Furthermore, $OtDUB_{275–675}$ was sufficient for binding AP-1/2 in both pulldown and peak-shift assays (Fig. 1E and F). Given that $OtDUB_{275–450}$ could not bind AP-1/2 and the structurally resolved GEF domain begins downstream at residue 548 (15), it is likely the C-terminal boundary for residues necessary for binding lies between 450 and 548.

AP complexes bind their cargo proteins through either dileucine-based (D/E-XXX-LL) or tyrosine-based motifs (YXXφ) located in the cargo proteins (17). Binding of tyrosine motifs occurs exclusively through the C-terminal domain of the mu subunit (μCTD) (18). To determine if OtDUB might utilize similar motifs for AP-1/2 association, peak-shift assays were first carried out with truncated AP-2 lacking the μ2CTD (Fig. 1G, AP-2-μ2CTD truncated) or with only the μCTD (Fig. 1H). OtDUB still bound to AP-2 lacking the μ2CTD and did not bind μCTD, suggesting AP-2 binding does not require a YXXφ in OtDUB. These data pointed to possible dileucine motif-based binding if OtDUB were to mimic a cargo protein in its binding to AP-1/2, and $OtDUB_{275–675}$ has four such consensus sequences. Circumstantial evidence supporting dileucine-motif binding is the NEM inhibition of binding from Fig. 1A. The AP-2 binding pocket for dileucine-based motifs contains a cysteine (19), which may be alkylated by NEM and could explain the loss of AP-1/2 binding to OtDUB in the presence of NEM (Fig. 1A).

The cytolysin listeriolysin O (LLO) from *Listeria monocytogenes* contains a PEST-like sequence that binds directly to the Ap2a2 subunit of AP-2, stimulating its endocytosis and removal from the host plasma membrane (20). This alternative AP-2 binding mechanism cannot be ruled out for $OtDUB_{275–675}$, although only two low-scoring PEST motifs in this region were predicted by the PESTfind algorithm. Given that effectors can bind AP-1/2 complexes either by occupying cargo docking sites or through alternative domains, further work will be needed to determine the mode of OtDUB binding to AP-1/2.

To assess if OtDUB and AP-1/2 associate in cells, various Flag-tagged OtDUB fragments were ectopically expressed in HeLa cells (Fig. 1I), immunoprecipitated from cell lysates, and assayed for Rac1, AP-1, and AP-2 association. Consistent with our proteomics data, Rac1 and AP-1/2 bound $OtDUB_{275–1369}$ but not $OtDUB_{675–1369}$ (15). The same minimal domain that bound AP-1/2 *in vitro*, $OtDUB_{275–675}$, also bound the complexes in cells (Fig. 1J). We conclude that $OtDUB_{275–675}$ is sufficient for direct AP-1/2 binding *in vitro* and in human cells.

Ectopic OtDUB expression disrupts endocytosis. The AP-2 adaptor complex mediates clathrin-dependent endocytosis by binding a cargo protein such as the transferrin receptor and recruiting downstream factors for plasma membrane invagination and vesiculation (16). To assess the impact of OtDUB on endocytosis, HeLa cells ectopically expressing the *Orientia* protein were pulsed with fluorescently labeled transferrin before being processed for wide-field fluorescence microscopy. Untransfected cells readily endocytosed the transferrin and the corresponding fluorescence signal was visible on interior endosomal structures in 93% $\pm$ 6% of these cells (n = 8; 765 total cells), which served as an internal control for endocytic activity on each coverslip (Fig. 2A). Expression of full-length OtDUB in transient

FIG 1 Legend (Continued)
GST-OtDUB or GST alone evaluated for enrichment by glutathione-resin pulldowns from bacterial lysates spiked with purified AP-1 or AP-2 core (n = 1). Eluates were resolved by SDS-PAGE and analyzed by immunoblotting or Ponceau-S staining (PonS). (E) Pulldown performed as in panel D with $OtDUB_{250–450}$ and $OtDUB_{275–675}$ being tested compared to controls (n = 1). For both D and E, representative Ponceau-S stains are used for the AP-1 and AP-2 pulldowns. (F, G, and H) Superose 6 gel filtration chromatograms of purified protein complexes. (F) AP2 core alone (green), $OtDUB_{275–675}$ alone (black dashed), or the complex of both (blue) (n = 1). (G) OtDUB alone (black) or in complex with AP-2-μ2CTD-truncated (blue) (n = 1). (H) AP2 μ2CTD alone (green), OtDUB alone (black), or (blue) (n = 1). The same representative OtDUB alone chromatogram is used in panels B, C, G, and H. (I) Cartoon representation of the OtDUB fragments used in panel J. (J) Ectopically expressed Flag-tagged OtDUB fragments were immunoprecipitated from HeLa cell lysates, resolved by SDS-PAGE with input lysates and immunoblotted for AP-1 (AP1G1) and AP-2 (AP2M1) subunits and the positive control Rac1 (n = 2). mAU, mean arbitrary units; FL, full length; GEF, guanine nucleotide exchange factor; UBD, ubiquitin-binding domain.

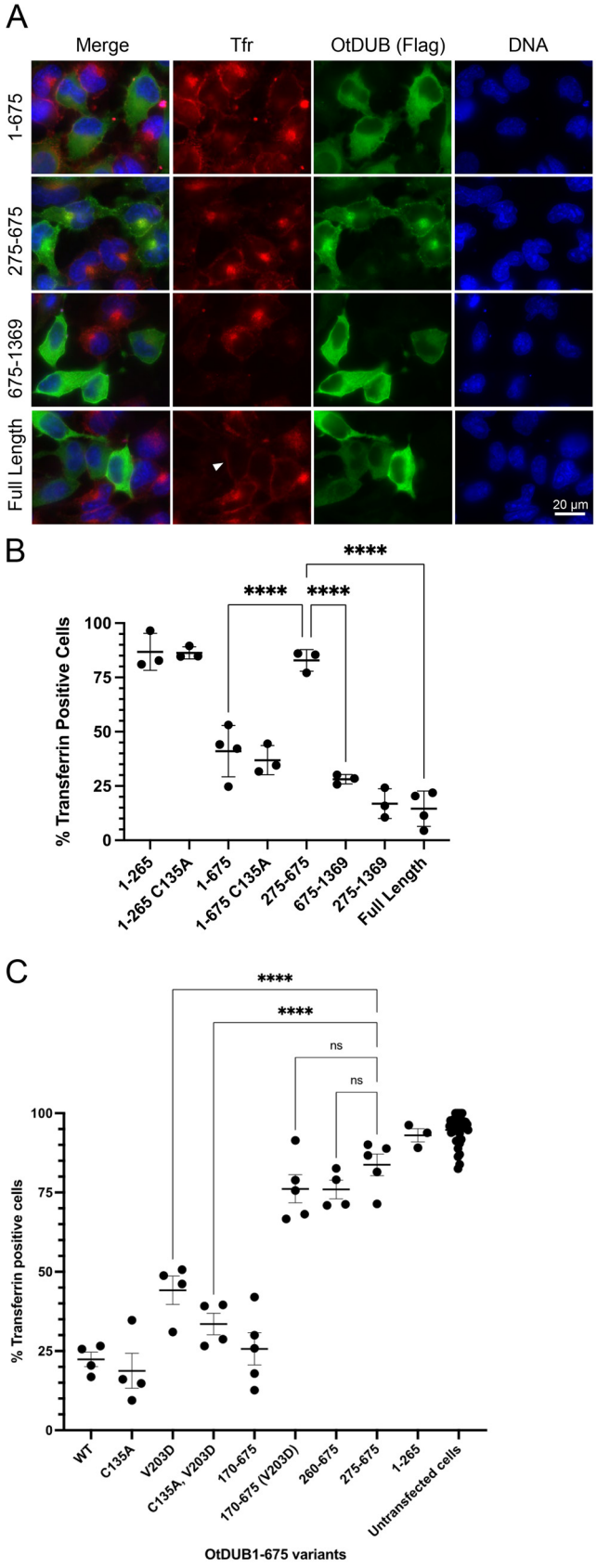

FIG 2 Endocytosis inhibition by OtDUB fragments with and without the AP1/2BD. (A) Representative images of HeLa cells ectopically expressing the indicated OtDUB-Flag fragments were incubated with fluorescently

(Continued on next page)

transfectants severely impacted endocytosis, with only 15% ± 8% of cells having internalized transferrin (Fig. 2A and B). A subset of OtDUB-expressing cells exhibited detectable enrichment of transferrin at the plasma membrane, suggesting the transferrin receptor is present and binding transferrin but is not being endocytosed in those cells (Fig. 2A, arrowhead). Other cells have no detectable transferrin at the plasma membrane, and this may indicate the receptor is not present due to defects in forward trafficking or endosome recycling.

To determine which OtDUB domain(s) was required for disrupting endocytosis, various ectopically expressed OtDUB fragments were tested. Two fragments containing the AP-1/2BD impaired endocytosis, with transferrin being internalized in only 17% ± 7% of $OtDUB_{275–1369}$-expressing cells and 41% ± 12% of $OtDUB_{1–675}$-expressing cells (Fig. 2A and B). Unexpectedly, the domain sufficient for AP-1/2 binding (AP-1/2BD) had only a marginal and statistically insignificant impact on endocytosis with 83% ± 5% of $OtDUB_{275–675}$-expressing cells containing transferrin. The $OtDUB_{1–265}$ DUB-UBD fragment did not significantly affect endocytosis: transferrin was internalized in 87% ± 9% of cells with the wild-type (WT) fragment and 89% ± 7% of cells with the DUB-inactive C135A derivative. The longer DUB-inactivated $OtDUB_{1–675}$-C135A fragment did still cause a significant decrease in transferrin-positive cells (37% ± 7%), suggesting the UBD (but not the activity of the DUB domain) when linked to the AP-1/2BD interferes in a dominant negative manner with endocytosis. Since residues 275–675 alone did not block endocytosis, but 275–1369 did, we tested $OtDUB_{675–1369}$ and found only 28% ± 2% of expressing cells had internalized transferrin (Fig. 2A and B). This fragment lacks the AP-1/2BD. Overall, the deletion analysis indicated that two domains of OtDUB are capable of blocking clathrin-mediated endocytosis: one resides in the $OtDUB_{1–675}$ segment that contains the AP-1/2BD and the other is in $OtDUB_{675–1369}$, which cannot bind AP-1/2.

To examine the contribution of the UBD within the context of $OtDUB_{1–675}$ in blocking endocytosis, we analyzed a number of $OtDUB_{1–675}$ variants and truncations thereof for their ability to take up transferrin (Fig. 2C). To our initial surprise, both $OtDUB_{1–675}$ with a V203D mutation, which strongly interferes with UBD-ubiquitin binding (12), and the C135A, V203D double mutant derivative still significantly impaired endocytosis compared to control cells expressing $OtDUB_{275–675}$. We hypothesized this might be due to ubiquitin binding by the active or inactive DUB domain (21). Indeed, only when the DUB domain was completely removed ($OtDUB_{170–675}$) was the UBD-dependent block to endocytosis eliminated: neither $OtDUB_{170–675}$-V203D nor $OtDUB_{260–675}$ significantly altered transferrin uptake compared to $OtDUB_{275–675}$ (Fig. 2C). Given these findings, it appears that strong ectopic expression of the AP-1/2BD of OtDUB tethered to a domain capable of binding ubiquitin interferes with endocytosis; whether this effect is relevant to the function of OtDUB expressed at normal levels remains uncertain (see Discussion).

The TGN is disrupted by $OtDUB_{675–1369}$, which overlaps a domain toxic to yeast. In addition to evaluating AP-2-dependent endocytosis, we analyzed cellular AP-1 activity by following the TGN marker cation-independent mannose-6 phosphate receptor (M6PR), which concentrates in the TGN and binds to lysosomal hydrolases to facilitate their AP-1-dependent transport to lysosomes (22). OtDUB-expressing cells exhibited a loss of M6PR-enriched foci, instead displaying a diffuse M6PR signal throughout the cytosol by immunofluorescence microscopy (Fig. 3A). By an OtDUB fragment analysis analogous to that carried out for transferrin uptake, we saw TGN disruption was independent of the AP-1/2BD but was observed with $OtDUB_{675–1369}$ (Fig. 3A and B).

FIG 2 Legend (Continued)
labeled transferrin (Tfr; red) for 15 min prior to fixation. Cells were then stained with anti-Flag antibodies (green) and Hoechst DNA stain (blue). Scale bar = 20 μm. (B) Quantification of fluorescent transferrin uptake by HeLa cells ectopically expressing different OtDUB-Flag fragments (a subset shown in panel A). Each data point represents quantification from an independent experiment (n = 3–4) for ≥211 total cells counted per condition. Horizontal bars and ranges represent means ± SD. ****, $P < 0.0001$, by ordinary one-way ANOVA with Tukey's multiple comparisons. (C) Quantification of fluorescent transferrin endocytosis in HeLa cells ectopically expressing $OtDUB_{1–675}$-Flag derivatives. Each data point represents quantification from an independent experiment for ≥216 total cells counted per condition. Horizontal bars and ranges represent means ± SE. ****, $P < 0.0001$, by one-way ANOVA test with Tukey's multiple comparisons as *post hoc* analysis.

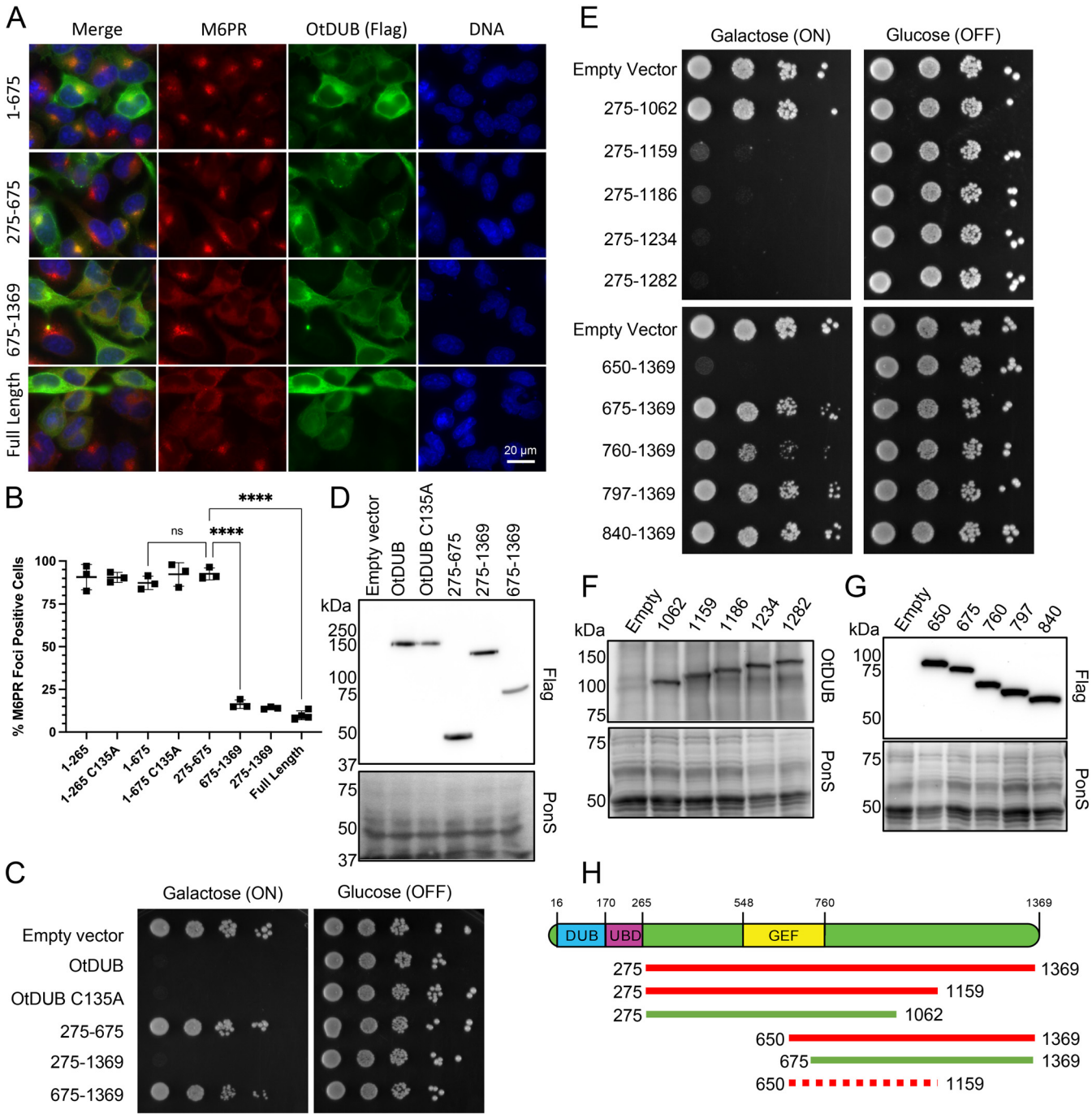

FIG 3 $OtDUB_{675–1369}$ disrupts the *trans*-Golgi network (TGN) and closely overlaps the minimal yeast toxicity domain $OtDUB_{650–1159}$. (A) Representative images of HeLa cells ectopically expressing the indicated OtDUB-Flag fragments were analyzed by indirect immunofluorescence with anti-Flag (green) and anti-M6PR (red) antibodies and Hoechst DNA stain (blue). Scale bar = 20 μm. (B) Quantification of focal localization of M6PR signal in HeLa cells ectopically expressing different OtDUB-Flag fragments (a subset shown in panel A). Each data point represents quantification from an independent experiment (n = 3–4), each with ≥219 total cells counted. Horizontal bars and ranges represent means ± SE; ns, not significant. ****, $P < 0.0001$, by ordinary one-way ANOVA with Tukey's multiple comparisons. (C) Growth analysis of wild-type (WT) yeast (W303) transformed with the empty p416GAL1 vector or expressing the indicated OtDUB-Flag fragments from the *GAL1* promoter. Cultures were serially diluted, spotted on galactose or glucose plates lacking uracil and grown for 3 days at 30°C (n = 2). (D) Steady state protein levels of OtDUB fragments from transformants in (C) were examined by anti-Flag immunoblot analysis of OtDUB-Flag proteins and Ponceau S staining for overall loading. (E) Growth assay performed as in (C) (n = 2). (F, G) Steady-state levels of OtDUB fragments from transformants in (E) were examined by anti-OtDUB immunoblotting of OtDUB-Flag fragments (F) or by anti-Flag immunoblotting (G). Ponceau S staining was used to compare loading. (H) Cartoon schematic of OtDUB and key OtDUB fragments analyzed for yeast toxicity. Nontoxic domains (green), toxic domains (red) and the inferred minimal toxicity domain, $OtDUB_{650–1159}$ (dashed red).

As previously reported, OtDUB inhibits yeast growth even in the absence of the DUB and UBD domains ($OtDUB_{275–1369}$) (15). However, neither subdomain $OtDUB_{275–675}$ nor $OtDUB_{675–1369}$ exhibited toxicity, suggesting residue 675 resides within the toxic domain (Fig. 3C and D). Residue 675 falls within the characterized GEF domain $OtDUB_{548–760}$, whose activity is also not responsible for toxicity (15). To hone in on the boundaries responsible for toxicity, we generated N- and C-terminal truncations of $OtDUB_{275–1369}$. C-terminal truncations of $OtDUB_{275–1369}$ were made roughly every 30–100 residues based on secondary structure predictions. Toxicity was lost between $OtDUB_{275–1159}$ and $OtDUB_{275–1062}$ (Fig. 3E, F, and H).

Given the GEF domain boundaries, we first made N-terminal truncations starting at residue 760 (Fig. 3E, G, and H). $OtDUB_{760–1369}$ exhibited a mild toxicity, while further truncations were not toxic at all. The earliest N-terminal start point for complete toxicity was residue 650, which was chosen based on our structural knowledge of this region (15). $OtDUB_{675–1369}$, which is minimally toxic, starts within a helical bundle of the GEF domain and likely disrupts this N-terminal structure, while $OtDUB_{650–1369}$ has the entire bundle intact to provide structural support for the C-terminal toxic domain. Together, these data suggest $OtDUB_{650–1159}$ is the minimal domain required for strong toxicity in yeast (Fig. 3H).

Mutations that suppress OtDUB yeast toxicity rescue membrane trafficking defects. We next designed a genetic selection to identify missense mutations within $OtDUB_{650–1159}$ capable of suppressing OtDUB toxicity in yeast. To this end, we generated an in-frame fusion linking the OtDUB toxic domain to the N-terminus of the auxotrophic marker Ura3 (Fig. 4A). When reporter expression is induced with galactose in cells plated on minimal media lacking uracil, only yeast expressing a full-length nontoxic chimera should be capable of growing. We designed several constructs starting at residue 650 and ending between residues 1159 and 1282. Fusion of Ura3-HA to the end of $OtDUB_{650–1159}$ was no longer deleterious to growth under these selection conditions; by contrast, fusions in which the C-terminal end points of the OtDUB insert extended to residues 1234 or 1282 were highly toxic with the Ura3-HA appendage (Fig. 4B).

To introduce random mutations at low frequency, the plasmid p415GAL1-$OtDUB_{650–1282}$-URA3-HA was cleaved to remove *OtDUB* codons 805–1282 (Fig. 4A and C). In parallel, the plasmid was used as a template for PCR amplification of *OtDUB* codons 760–1282 and a 5′ portion of *URA3* (Fig. 4A). The screen was designed to generate mutations only between codons 760 and 1282, since any mutation between 650 and 760 would impact the GEF domain. The gapped plasmid and the PCR product were then cotransformed into yeast for gap repair by homologous recombination (Fig. 4C). Single colonies from the selective growth plates were isolated, and plasmids were recovered for Sanger sequencing. From 4 independent transformations, 94 total plasmids were recovered; 43 contained single amino acid mutations at 24 different positions (42 of which occurred between residues 760 and 1159) (Fig. 4D). All but 1 of the 43 mutations (A1206P) occurred within the boundaries of the OtDUB toxic domain ($OtDUB_{650–1159}$). Eighty percent of the mutations clustered within 110 residues (969–1079), which we call Zone 2. Zone 2 represented just 21% of the PCR product length, implicating it as a key region within the toxic domain. A smaller upstream cluster, representing 12% of the mutations, was dubbed Zone 1 (residues 824–885).

To validate these findings, recovered plasmids representing each of the 24 mutated residues were retransformed into yeast and tested for suppression; the C1053Y mutant plasmid is shown as an example (Fig. 4E). Evaluation of protein expression in a panel of these mutants showed steady-state levels comparable to those of the original $OtDUB_{650–1282}$-Ura3-HA protein (Fig. 4F).

Given the overlap of the yeast toxic domain ($OtDUB_{650–1159}$) and the domain responsible for membrane trafficking defects ($OtDUB_{675–1369}$), we wondered if these mutations could suppress the Golgi disruption caused by $OtDUB_{675–1369}$ in HeLa cells. Eleven of the 24 mutation sites were selected based on their position and frequency (Fig. 4D, bold), and these mutations were introduced into the $OtDUB_{675–1369}$ mammalian expression vector. HeLa cells ectopically expressing these proteins were assessed by indirect immunofluorescence for the localization of the *cis*-Golgi marker GM130. In control $OtDUB_{275–675}$ (AP-1/2 BD)-expressing cells, 90% $\pm$ 5% of cells had a compact Golgi focal structure (Fig. 4G and H). By contrast, only

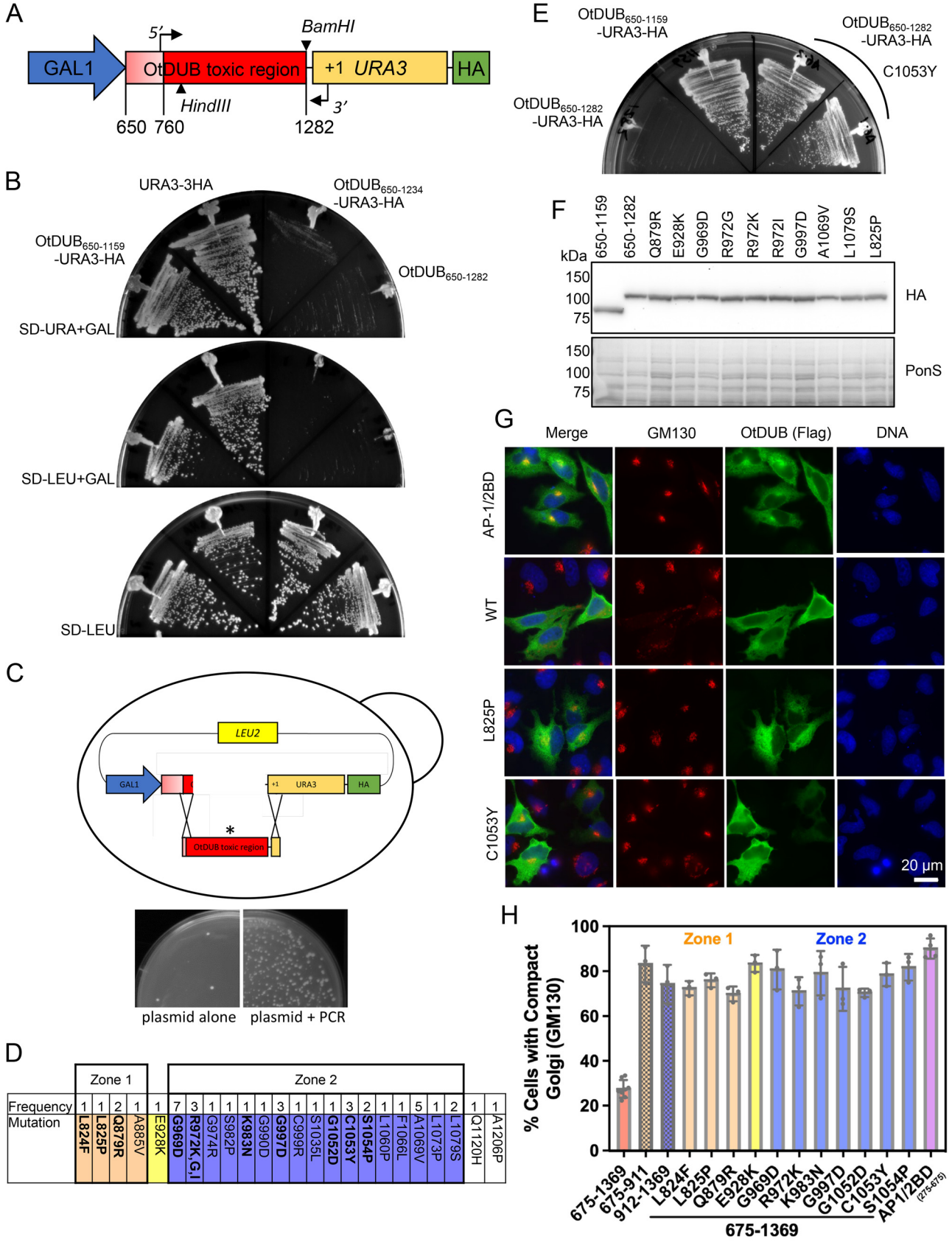

FIG 4 OtDUB yeast toxicity and Golgi disruption in human cells are suppressed by the same point mutations. (A) Schematic of the galactose-inducible gene fusion used to select for suppressing mutations in the OtDUB toxic region. Codons 650–1282 were cloned in-frame with *URA3* and a C-terminal

(Continued on next page)

28% ± 4% of cells expressing $OtDUB_{675–1369}$ exhibited a compact Golgi structure; the remaining 72% of these cells showed a dispersed or fragmented GM130 signal (Fig. 4G and H).

Representative images of $OtDUB_{675–1369}$ proteins with Zone 1 (L825P) or Zone 2 (C1053Y) mutations are shown in Fig. 4G; both lost the Golgi fragmentation defect. In fact, each of the tested yeast toxicity suppressor mutations was able to significantly restore WT Golgi structure to $OtDUB_{675–1369}$-expressing cells, with 67–82% of cells exhibiting compact Golgi structures (Fig. 4H). We also assessed whether OtDUB fragments containing only Zone 1 or Zone 2 alone could disrupt the Golgi, using $OtDUB_{675–911}$ and $OtDUB_{912–1369}$, respectively. Neither fragment significantly disrupted the Golgi (Fig. 4H), suggesting both zones are required for Golgi disruption just as they are both required for yeast toxicity. Cumulatively, these data directly link the $OtDUB_{650–1159}$ toxicity in yeast to the disrupted membrane trafficking phenotype in cultured human cells observed with $OtDUB_{675–1369}$.

The yeast toxicity domain of OtDUB binds phosphatidylserine and alters its localization. In characterizing the effects of OtDUB on AP-1/2 functions, we noticed that $OtDUB_{675–1369}$ frequently localizes at or near the plasma membrane (see Fig. 2A and Fig. 3A). None of our proteomic protein-interaction data had linked this fragment of OtDUB to the plasma membrane. Since GEF domain-containing proteins frequently have a phospholipid-binding pleckstrin homology (PH) domain to localize the GEF near its cognate GTPase (23), we decided to test OtDUB for lipid binding. Using a protein-lipid overlay assay with recombinant full-length $OtDUB_{C135A}$ and commercially available lipid-spotted filters, we screened 22 unique lipids across 2 filters containing an overlapping set of lipids (Fig. 5A). On both filters, OtDUB bound specifically to phosphatidylserine (PS).

To validate the PS binding observed in the overlay assay, we performed liposome cosedimentation assays using OtDUB fragments and liposomes containing 0% or 30% PS. The $OtDUB_{275–1369}$ and $OtDUB_{675–1369}$ fragments were substantially enriched in the pelleted 30% PS liposomes compared to their 0% PS counterparts, whereas $OtDUB_{275–675}$ showed no enrichment (Fig. 5B). Given that the PS-binding domain is within OtDUB residues 675–1369 and this overlaps with the segment displaying yeast toxicity, we tested two toxicity suppressor mutations for loss of PS binding. Using the protein-lipid overlay assay, recombinant GST-$OtDUB_{275–1369}$ displayed strong PS binding, while the Q879R and C1053Y mutants showed minimal binding (Fig. 5C). These data suggest OtDUB directly binds the acidic PS lipid head group and does so through the domain responsible for disrupting membrane trafficking in human cells and causing toxicity in yeast.

To test if PS is required for OtDUB yeast toxicity, we expressed $OtDUB_{650–1282}$-URA3-HA in *cho1*Δ yeast, a strain devoid of PS (24). WT and *cho1*Δ yeast transformants carrying $OtDUB_{650–1282}$-URA3-HA, $OtDUB_{650–1282}$-URA3-HA-C1053Y, or empty vector were serially diluted and spotted on minimal medium lacking leucine, supplemented with choline and ethanolamine to support *cho1*Δ growth and with glucose or galactose as a carbon source. When $OtDUB_{650–1282}$-URA3-HA expression was induced in *cho1*Δ cells, no growth defect was observed, while it inhibited growth completely in WT control cells (Fig. 5D); expression of the protein was comparable in the two strains (Fig. 5E). Growth inhibition of WT yeast in

FIG 4 Legend (Continued)
HA epitope coding sequence. PCR primers annealing at codon 760 (5′) and within *URA3* (3′) were used to amplify the toxic region with infrequent nucleotide changes. The plasmid was gapped with the HindIII and BamHI enzymes. (B) Growth of cells with gene fusions of the indicated *OtDUB* fragments and *URA3* expressed from the p415GAL1 (*LEU2*) vector were compared to a *URA3-3HA* control by streaking onto a galactose plate lacking uracil (top), a galactose plate lacking leucine (middle) or a glucose plate lacking leucine (bottom) for 2–4 days at 30°C. (C) Cartoon of gap repair method in yeast; linearized plasmid and PCR amplicon were cotransformed into yeast and repaired by homologous recombination, * denotes mutant transcript (top). Comparison of cells transformed with gapped plasmid alone or in combination with the PCR amplicon followed by plating on minimal media lacking leucine (bottom). (D) The location and frequency of single-site mutations recovered from the selection for OtDUB toxic domain suppressors. (E) Representative experiment for the retransformation of recovered and sequenced plasmids containing single missense mutations. Two independent p415GAL1 $OtDUB_{650–1282}$-C1053Y transformants were struck out on galactose-containing minimal media lacking uracil along with $OtDUB_{650–1159}$ and $OtDUB_{650–1282}$ as controls and grown at 30°C for 3 days. (F) A subset of recovered plasmid transformants were grown in galactose media lacking leucine and extracts from 0.25 OD_{600} units of cells were resolved by SDS-PAGE and immunoblotted with anti-HA antibodies. Ponceau S staining used for loading comparison (n = 1). (G) Representative indirect immunofluorescence images visualizing the *cis*-Golgi with GM130 staining (red), in HeLa cells transiently expressing OtDUB-Flag fragments (green). Scale bar = 20 μm. One Zone 1 mutant (L825P) and one Zone 2 mutant (C1053Y) are compared to WT $OtDUB_{675–1369}$ and the negative control AP-1/2BD ($OtDUB_{275–675}$). (H) Quantification of HeLa cells ectopically expressing $OtDUB_{675–1369}$ mutant variants exhibiting a compact (WT) GM130 staining pattern (from micrographs similar to panel G). Each data point represents a technical replicate ($n \geq 3$, total cells quantified is ≥90). The bars represent means ± SD.

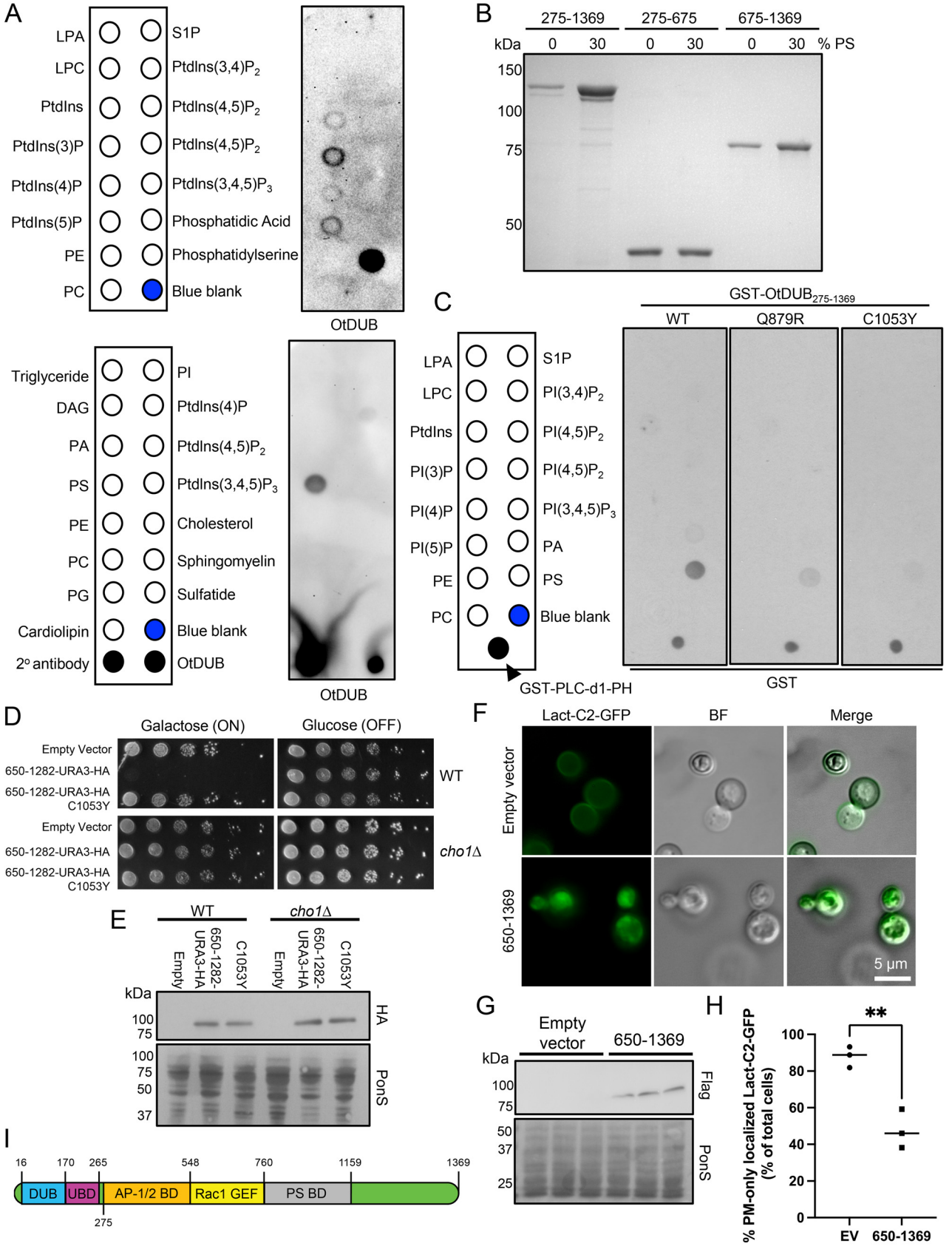

FIG 5 OtDUB binds phosphatidylserine and binding involves residues also required for membrane trafficking defects. (A) Protein-lipid overlay screening was performed on commercially available hydrophobic membranes spotted with the indicated lipids by adding 0.5 µg/mL of recombinant

(Continued on next page)

the presence of choline and ethanolamine suggests OtDUB yeast toxicity is not driven by PS depletion. The strong genetic link between OtDUB yeast toxicity and the presence of PS provide evidence for OtDUB-PS binding *in vivo*.

To further characterize the OtDUB PS-binding domain, we coexpressed $OtDUB_{650–1282}$-URA3-HA with the PS sensor Lact-C2-GFP in yeast (25). The Lact-C2-GFP sensor binds PS and localizes strongly to the plasma membrane as observed when cotransformed with empty vector (Fig. 5F). When expressed with $OtDUB_{650–1369}$ (Fig. 5G), the Lact-C2-GFP plasma membrane signal is greatly reduced and becomes dispersed within the cell (Fig. 5F). The number of cells with plasma membrane GFP signal is reduced by roughly 2-fold in the presence of $OtDUB_{650–1369}$ (Fig. 5H). While the sensor localization change is striking, it is unknown how OtDUB-PS binding causes the change. Nevertheless, this redistribution of PS within the cell supports an important role for OtDUB-PS interaction in membrane alterations by the *Orientia* protein.

DISCUSSION

Our efforts to characterize the OtDUB protein from the *Orientia tsutsugamushi* pathogen have uncovered a multitude of biochemical activities that likely modulate host cell activities. Previously, we discovered and characterized a deubiquitylase (DUB), a high-affinity UBD, and a novel Rac1 GEF domain (12, 15). Here we present data for two additional biochemical activities: a domain sufficient for binding the clathrin adaptor protein complexes AP-1 and AP-2, and a region that binds the PS phospholipid and disrupts membrane trafficking.

Apparent interactions with AP-1 and AP-2 were originally identified in a proteomic screen for OtDUB-host protein interactions (15). We validated these interactions here through direct binding and immunoprecipitation experiments; our data indicate binding is mediated by elements within $OtDUB_{275–675}$, but the exact boundaries are still unknown (Fig. 5I). Interestingly, while endocytosis and TGN trafficking were both disrupted in cells ectopically expressing full-length OtDUB, $OtDUB_{275–675}$ alone had no effect on either pathway. Potentially, OtDUB interaction with AP-1/2 may tether OtDUB to specific membranes to modulate trafficking pathways by other domains of the *Orientia* protein. For example, when $OtDUB_{1–675}$ is ectopically expressed in HeLa cells, it disrupts endocytosis, and this effect requires the ubiquitin-binding capabilities contributed by either the UBD or DUB domain.

This ubiquitin-binding requirement for disrupting endocytosis suggests OtDUB may take advantage of known effects of monoubiquitination on endocytic mechanisms. It could do so by binding ubiquitin through the high-affinity UBD or carrying out coupled monoubiquitination via the UBD. Monoubiquitination of endocytic cargo proteins is a common modification and is required for efficient endocytic activity (26). Under ectopic expression conditions, ubiquitin binding by $OtDUB_{1–675}$ may be causing dominant negative effects on endocytosis. In the context of *Orientia* infections, the levels of OtDUB will likely be far lower than during transient expression in HeLa cell transfectants. Hence, the ability of OtDUB to bind ubiquitin and AP-1 or AP-2 could induce localized membrane remodeling that may differ from the dominant effect on endocytosis seen here.

FIG 5 Legend (Continued)
$OtDUB_{C135A}$-Flag followed by immunoblotting for OtDUB with anti-OtDUB antibodies ($n = 1$). As positive controls, one membrane was spotted with 1 µL of secondary antibody and with 100 ng of $OtDUB_{C135A}$-Flag. (B) Liposome sedimentation assay pellets from liposomes containing 0% or 30% phosphatidylserine (PS) incubated with 4 µM the indicated recombinant OtDUB polypeptide fragments were resolved by SDS-PAGE and stained ($n = 3$). (C) Protein-lipid overlays were carried out using 2 µg/mL of the indicated GST-$OtDUB_{275–1369}$ variants followed by immunoblotting with anti-GST antibodies ($n = 1$). As a positive control, 500 pg of GST-PLC-d1-PH protein were spotted on each membrane. (D) WT or *cho1Δ* transformants carrying p415GAL1, p415GAL1-$OtDUB_{650–1282}$, or p415GAL1-$OtDUB_{650–1282}$-C1053Y were serially diluted and plated on minimal media lacking leucine and supplemented with choline and ethanolamine, and containing either glucose or galactose. Cells were grown at 30°C for 2–6 days ($n = 3$). (E) Transformants from panel D grown in galactose were used to make extracts from 0.25 OD_{600} units; proteins were analyzed by anti-HA immunoblotting. Ponceau S staining was used for loading comparison ($n = 1$). (F) Epifluorescence images of the PS biosensor Lact-C2-GFP after galactose induced expression of $OtDUB_{650–1369}$ or empty vector. (G) The three transformants used for panels F and H were cultured to make extracts, and 0.25 OD_{600} units of cells were analyzed by anti-Flag immunoblotting. Ponceau S staining was used for loading comparison. (H) Quantification of yeast strains used in panel F. Each data point represents quantification from an independent transformant, 32–45 cells counted per transformant. (112 total control cells 143 total cells expressing $OtDUB_{650–1369}$). Horizontal bars represent the mean. **, $P < 0.01$, by Student's *t* test. (I) Cartoon representation of OtDUB with current boundaries mapped for each known functional domain. The exact boundaries of AP-1/2BD and the N-terminal boundary of PS-BD remain unknown. BF, bright field; EV, empty vector; DAG, diacylglycerol; LPA, lysophosphatidic acid; LPC, lysophosphatidylcholine; PA, phosphatidic acid; PE, phosphatidylethanolamine; PC, phosphatidylcholine; PS, phosphatidylserine; PG, phosphatidylglycerol; PI, phosphatidylinositol; SP-1, sphingosine-1-phosphate; PtdIn(x)P, phosphatidylinositol (X) phosphate.

Unexpectedly, an OtDUB fragment that does not bind AP-1/2 is capable of strongly impairing both endocytosis and TGN trafficking: $OtDUB_{675–1369}$ not only interferes with endocytosis and the TGN but also disrupts the *cis*-Golgi, suggesting its ectopic expression causes general imbalances in membrane trafficking homeostasis. Future studies will be needed to elucidate the exact stage(s) of trafficking being impacted. It is noteworthy that $OtDUB_{675–1369}$ also contains most of the region (residues 650–1159) responsible for very strong toxicity in yeast, suggesting the same domain may be responsible for both disruption of membrane trafficking and inhibited yeast growth. We initially searched for conserved primary and tertiary structure features in this region but did not find any. This is not surprising given that the UBD, the GEF domain, and the AP1/2BD (identified in this study) were also not revealed by primary sequence searches. We did not identify any proteins bound to the C-terminal half of OtDUB that would suggest any relevance to the above phenotypic effects.

We therefore used a selection based on yeast growth to identify single-residue missense mutations capable of suppressing $OtDUB_{650–1282}$ toxicity (Fig. 4). These same mutations also suppress the Golgi fragmentation caused by $OtDUB_{675–1369}$ in HeLa cells, indicating the same domain is responsible for both traits. We eventually linked a biochemical activity to this domain by screening for phospholipid binding. $OtDUB_{675–1369}$ binds directly and specifically to the anionic lipid PS. Furthermore, two mutants identified in the yeast suppressor screen (Q879R and C1053Y) almost completely blocked PS binding *in vitro*, suggesting the trafficking defects in human cells and toxicity in yeast are due to PS binding (Fig. 5I). To complement the biochemical data, we found $OtDUB_{650–1282}$ has no toxicity when expressed in a yeast strain lacking PS (*cho1*Δ). Furthermore, the localization of the PS biosensor Lact-C2-GFP is diverted from the plasma membrane in yeast expressing high levels of $OtDUB_{650–1369}$. Together, these data provide strong evidence for *in vivo* PS binding by OtDUB.

Two basic residues that were found to be mutated in the screen (R972 and K983) could be at least partially responsible for providing the PS head-group binding site. One mutation of K983 (to N) and three mutations of R972 (to K, G, and I) were identified. The R972K mutation is a conservative change, but the arginine side chain is more basic and could bind the anionic headgroup of PS more readily. The remaining mutated residues may be required for folding or structural stability of the PS-binding domain. The PS-binding activity observed here could function together with the nearby Rac1 GEF domain. Lipid binding, often involving PH domains, is a commonly observed feature of GEF proteins (23). Positioning of the OtDUB GEF domain at the plasma membrane may allow localized exchange of GDP for GTP on Rac1 and might also enhance GEF activity.

Potentially, this OtDUB domain not only binds PS but also has a lipid transport activity or can modify the lipid enzymatically. Other PS-binding domains, such as the C2 domain from Lactadherin, which binds PS with nanomolar affinity, and the PH domain of Evt-2, have been ectopically expressed without inhibiting growth in yeast or disrupting Golgi structure in mammalian cells (27, 28). While PS is known to be essential in mammalian cells, the exact PS functions that OtDUB is disrupting are currently unclear (29). The OtDUB PS-binding domain may prove to be a useful tool for better understanding the role of PS in healthy, nonapoptotic cells. While beyond the scope of this study, an in-depth analysis of cellular lipid content could address the relative PS levels in the presence of exogenous OtDUB in yeast and mammalian cells.

PS binding could help localize OtDUB protein to the plasma membrane, endosomes, and/or the TGN where PS is concentrated (29). Plasma membrane localization of OtDUB while binding AP-2 might promote AP-2 binding to membrane domains enriched in phosphatidylinositol-4,5-bisphosphate and activate AP-2 (30, 31). Similarly, OtDUB-bound AP-1 could simultaneously interact with phosphatidylinositol-4-phosphate, which is enriched in endosomes and the TGN, and result in AP-1 activation, at least when in the presence of the GTPase Arf1, a second cofactor required for AP-1 activation (31, 32).

A well-characterized role for PS occurs during cell apoptosis. In cells undergoing apoptosis, PS relocalizes from the inner leaflet to the outer leaflet of the plasma membrane, and this surface charge change leads to the recruitment of phagocytes and eventual clearance of the apoptotic cell (33). During *Orientia* infection there is evidence for both pro- and antiapoptotic

activities, depending on the strain of *Orientia* and the infected cell type analyzed (3). A potential function of the OtDUB PS-binding domain during infection would be to prevent PS relocalization to the outer membrane to suppress apoptosis and allow for the persistence of infection. Another possible role during infection would be to localize OtDUB to the host plasma membrane to locally activate Rac1 via the OtDUB GEF domain, which appears to contribute to actin-dependent changes in cellular architecture (15).

Interestingly, the effector protein CagA from the pathogenic bacterium *Helicobacter pylori* is also a PS-binding protein and is a known surface protein of the bacterium. *H. pylori* gains entry into host cells following contact-dependent flipping of inner leaflet PS to the outer leaflet of the plasma membrane, which allows CagA-PS binding and initiation of bacterial internalization (34). If OtDUB is a surface protein of *Orientia*, the PS-binding domain could have a similar function in host cell entry. Future work examining the roles of OtDUB and its different domains during *Orientia* infection will be needed to resolve these questions.

MATERIALS AND METHODS

Plasmids. All plasmids and primers used in this study are in Table 1, and the plasmids were generated using standard cloning techniques. Plasmids were confirmed by sequencing and/or restriction analysis (12, 15, 32, 35, 36).

Protein purifications. For purifications of OtDUB tagged with both glutathione *S*-transferase (GST) and a Flag epitope, Rosetta DE3 *E. coli* transformed with pGEX6P-1-OtDUB-Flag (WT or C135A) were back-diluted in Luria-Bertani (LB) medium supplemented with 100 μg/mL of ampicillin, grown at 37°C, induced with 300 μM isopropyl β-D-1-thiogalactopyranoside (IPTG) at an optical density at 600 nm (OD_{600}) of 0.5–0.6, and incubated at 18°C for 16 h. Harvested cells were pelleted and resuspended in ice-cold phosphate-buffered saline (PBS) containing 400 mM KCl, 1 mM DTT, 2 mM PMSF, lysozyme, DNase. After incubating on ice for 1 h, cells were lysed at 900 lbs of pressure in a French press and centrifuged at 50,000 $\times$ *g* to remove insoluble material.

Clarified lysates were loaded onto a glutathione resin (17513202; Cytiva) gravity column preequilibrated with wash buffer (PBS + 400 mM KCl). After extensive washing, proteins were eluted with 250 mM Tris-HCl pH 8, 0.5 M KCl, and 10 mM reduced glutathione. Eluates were then incubated with GST-human rhinovirus (HRV) 3C protease during a 2-stage dialysis: first in wash buffer + 1 mM DTT and then in wash buffer. The cleaved and dialyzed protein was then concentrated using an Amicon Ultra 50 kDa cutoff filter (UFC905024; Sigma) and further dialyzed in Flag buffer (50 mM Tris-HCl pH 7.5, 150 mM NaCl) before being loaded onto a column with 0.5 mL preequilibrated M2 Flag resin (A2220; Sigma). The column was washed with 20 mL of Flag buffer supplemented with 0.1% Tween 20, and the OtDUB protein was eluted with 1.5 mL of Flag buffer + 0.2 μg/mL 3xFlag peptide. Finally, eluates were resolved by size exclusion fast protein liquid chromatography (ÄKTA) on a Superose-6 column equilibrated with 50 mM HEPES pH 7.5, 100 mM NaCl. Peak fractions were analyzed by SDS-PAGE and GelCode Blue (24590; ThermoFisher) staining, and fractions containing full-length OtDUB were pooled and concentrated to ~1 mg/mL as determined by A_{280}. Aliquots were flash frozen in liquid N_2 and stored at −80°C.

$OtDUB_{275–675}$ was purified as was done for the full-length protein but with the following changes. After overnight dialysis, the free GST tag and GST-HRV 3C protease were recaptured on glutathione resin and the flow through was concentrated and loaded onto a Superdex75 HiLoad column preequilibrated with 25 mM HEPES, 5 mM Tris-HCl pH 8.0, 200 mM NaCl, and 1 mM DTT. Peak fractions were pooled and concentrated. The protein concentration was determined by A_{280}, aliquoted, flash frozen in liquid N_2, and stored at −80°C.

For purification of GST-$OtDUB_{275–1369}$ (WT, Q879R, and C1053Y) proteins, clarified lysates were incubated with glutathione resin for 1 h at 4°C, and the resins were washed extensively with wash buffer (PBS + 400 mM KCl). After washing, GST-tagged proteins were eluted with 10 mL of elution buffer (250 mM Tris-HCl pH 8, 0.5 M KCl, and 10 mM reduced glutathione), and the eluted proteins were subject to a buffer change to 50 mM HEPES pH 7.5, 150 mM NaCl buffer using an Amicon Ultra 3 kDa cutoff filter (UFC900324, Sigma) following the manufacturer's protocol. The concentrated proteins were loaded onto a Superdex 200 gel filtration column preequilibrated with 50 mM HEPES pH 7.5, 150 mM NaCl. Protein concentrations were determined by Bradford assay (5000205; Bio-Rad). All proteins were flash-frozen in liquid N_2 and stored at −80°C until use.

AP-1 core was purified as previously published with minor adjustments (32). Rosetta DE3 cells transformed with a plasmid coding for all four subunits (AP-1 core/pST39) (32) were back diluted in LB containing 100 μg/mL ampicillin and grown at 37°C. Protein expression was induced at OD_{600} 0.5–0.6 with 300 μM IPTG and the culture was shifted to 20°C for 16 h. After centrifuging the culture, the resulting bacterial pellet was resuspended in AP-1 lysis buffer (50 mM Tris-HCl pH 8.0, 300 mM NaCl, 10% glycerol, 3 mM β-mercaptoethanol [βME], 2 mM PMSF, lysozyme, DNase) and incubated on ice for 1 h. Cells were mechanically disrupted with 900 lbs. pressure in a French press and centrifuged at 50,000 $\times$ *g* to pellet the insoluble fraction. Clarified lysates were incubated with 5 mL of Ni-NTA resin (30210; Qiagen), and AP-1 core was batch purified by rotating for 1 h at 4°C. The sample was transferred to a 25-mL gravity column, and the settled resin was washed with wash buffer (50 mM Tris-HCl pH 8.0, 300 mM NaCl, 10% glycerol, 3 mM βME) before elution with wash buffer containing 250 mM imidazole, pH 8.0. The eluate was then loaded onto 3 mL of packed glutathione resin in a 25 mL gravity column. The resin was handled similarly to the Ni-NTA resin, and the protein was eluted with 250 mM Tris-HCl pH 8.0, 200 mM NaCl, 3 mM βME, and 10 mM reduced glutathione. Overnight tag cleavage was performed with 6×His-TEV protease during dialysis in column buffer (20 mM Tris-HCl pH 8.0, 200 mM NaCl, 1 mM DTT). The protein was then concentrated and loaded onto an S200 HiLoad column preequilibrated with column buffer and further purified by size exclusion chromatography. Main peak fractions were pooled and concentrated, and aliquots were flash

TABLE 1 List of plasmids, primers, and molecular cloning strategies used in this study

Plasmids	Plasmid name	Cloning notes	Primer name	Primer sequence
Bacterial plasmids				
1	pGEX6P1 GST-OtDUB (1-1369)-1xFlag	Previously published in Lim et al. (15)		
2	pGEX6P1 GST-OtDUB C135A (1-1369)-1xFlag	Site-directed mutagenesis of pGEX6P GST-OtDUB (1-1369)-1xFlag to generate C135A	JMB652	GTATGATGCTGGACCATTTGTGGTTGACAACCTGATC
			JMB653	GTCCAGCATCATACACGTTGGTTTGCTGAACTGTCTGC
3	pGEX6P1 GST-OtDUB (1-675)-1xFlag	Previously published in Lim et al. (15)		
4	pGEX6P1 GST-OtDUB (675-1369)-1xFlag	Previously published in Lim et al. (15)		
5	pGEX6P1 GST-OtDUB (275-1369)-1xFlag	Previously published in Lim et al. (15)		
6	pGEX6P1 GST-OtDUB (275-1369) Q879R-1xFlag	Site-directed mutagenesis of pGEX6P1 GST-OtDUB (275-1369)-1xFlag to generate Q879R	JMB819	GTTGCGGCCCGCCAAATGCTCTGCCCAAGCTTTGCTG
			JMB820	CGGGCCGCAACATTGCATCAGGCAGCTCGGAACAC
7	pGEX6P1 GST-OtDUB (275-1369) C1053Y-1xFlag	Site-directed mutagenesis of pGEX6P1 GST-OtDUB (275-1369)-1xFlag to generate C1053Y	JMB805	CAGGCTACTCAAGCGCCCCTCAAATTCTGATCAATATGCAC
			JMB806	GCTTGAGTAGCCTGGAATGAATTTGTCACCGGTCATGTTGGAAATGTCC
8	pGEX6P1 GST-OtDUB (275-675)	pCDNA3.1(+) OtDUB (1-1369)-1xFlag was used as template. The primers contain 5′-BamHI and 3′-XhoI restriction sites and a 3′-stop codon. The amplicon was digested and ligated into like cut pGEX6P1	J MB666	GTACGGATCCGCAAGCGCCGAAGTGTCTTCC
			JMB667	GTACCTCGAGTTAAAATGGGATTGCTCTCAGAG
9	pGEX6P GST-OtDUB (275-450)	Site-directed mutagenesis of pGEX6P1 GST-OtDUB (275-675)-1xFlag to introduce a stop codon at residue C451	JMB676	CATTCTGAAACATCATCGGTGCTAACGCTGTTAAGTTTTTCTCTCC
			JMB677	GATGTTTCAGAATGGATGTCTCTTTTCCTTCTGTTTCAGC
10	pGEX6P1 GST-OtDUB 1-1190	Site-directed mutagensis of L1161 to a stop codon in pGEX6P1 GST-OtDUB (1-1369) noncodon optimized DNA	JMB568	GTCTTAAAAAACAGAGCCAGATATTCAGAGTAGGG
			JMB569	GTTTTTTAAGACTTATTATCACTATTTTGAG
11	pGEX6P1 GST-OtDUB 1-911	Site-directed mutagensis of Y912 to a stop codon in pGEX6P1 GST-OtDUB (1-1369) noncodon optimized DNA	JMB570	GATAACTAAAAAAATAGCGGGACTGCACAATCAAAACGTG
			JMB571	GCTATTTTTTTAGTTATCAATTGCACAAAATACTCCTTG
12	pGEX6P1 GST-OtDUB 1-311	Previously published in Berk et al. (12)		
13	pGEX6P1 GST-OtDUB 1-265	Previously published in Berk et al. (12)		
14	pGEX6P1 GST-OtDUB 1-177	Previously published in Berk et al. (12)		
15	AP-1 core/pST39	Previously published in Ren et al. (32)		
16	pETDuet encoding human β2 (1-591) and human full-length μ2 (1-435)	Previously published in Kwon et al. (35)		
17	pETDuet encoding human β2 (1-591) and human CTD-truncated μ2 (1-135)	Previously published in Kwon et al. (35)		
18	pCDFDuet encoding rat α (1-621) with a C-terminal GST tag and human σ 2(1-142)	Previously published in Kwon et al. (35)		
19	pMAT9S human μ2 CTD (159-435)	Previously published in Kwon et al. (35)		
Mammalian plasmids				
20	pCDNA3.1(+) OtDUB (1-1369)-1xFlag	Previously published in Lim et al. (15)		
21	pCDNA3.1(+) OtDUB (1-1369) C135A-1xFlag	Previously published in Lim et al. (15)		
22	pCDNA3.1(+) OtDUB (1-675)-1xFlag	Previously published in Lim et al. (15)		
23	pCDNA3.1(+) OtDUB (1-675) C135A-1xFlag	pCDNA3.1(+) OtDUB (1-1369) C135A-1xFlag was used as template. The primers contain 5′-BamHI and 3′-XhoI restriction sites and a 3′-1xFlag-stop codon. The amplicon was digested and ligate d into like cut pCDNA3.1(+)	JMB672	GTACGGATCCACCATGGCAAACG
			JMB681	GTACCTCGAGTTATTTATCGTCATCATCTTTGTAATCGCCTGAGCC AAATGGGATTGCTCTCAGAG
24	pCDNA3.1(+) OtDUB (1-675) V203D-1xFlag	Site-directed mutagenesis of pCDNA3.1(+) OtDUB (1-675)-1xFlag to introduce the V203D mutation	CSL450	GGTGTGCTGGACGATAGAATCTTCGACAATAAGATTTTGTCCGTG
			CSL451	GATTCTATCGTCCAGCACACCCTCTGTGATTCTGTTGTTGTTC
25	pCDNA3.1(+) OtDUB (1-675) C135A V203D-1xFlag	Site-directed mutagenesis of pCDNA3.1(+) OtDUB (1-675) C135A-1xFlag to introduce the V203D mutation	CSL450	GGTGTGCTGGACGATAGAATCTTCGACAATAAGATTTTGTCCGTG
			CSL451	GATTCTATCGTCCAGCACACCCTCTGTGATTCTGTTGTTGTTC
26	pCDNA3.1(+) OtDUB (1-265)-1xFlag	pCDNA3.1(+) OtDUB (1-1369)-1xFlag was used as template. The primers contain 5′-BamHI and 3′-XhoI restriction sites and a 3′-1xFlag-stop codon. The amplicon was digested and ligated into like cut pCDNA3.1(+)	JMB672	GTACGGATCCACCATGGCAAACG
			JMB682	GTACCTCGAGTTATTTATCGTCATCATCTTTGTAA TCGCCTGAGCCGGATTTGTTGAACTTCTC
27	pCDNA3.1(+) OtDUB (1-265) C135A-1xFlag	pCDNA3.1(+) OtDUB (1-1369) C135A-1xFlag was used as template. The primers contain 5′-BamHI and 3′-XhoI restriction sites and a 3′-1xFlag-stop codon. The amplicon was digested and ligated into like cut pCDNA3.1(+)	JMB672	GTACGGATCCACCATGGCAAACG
			JMB682	GTACCTCGAGTTATTTATCGTCATCATCTTTGTAA TCGCCTGAGCCGGATTTGTTGAACTTCTC
28	pCDNA3.1(+) OtDUB (170-675)-1xFlag		MZ276	GTACGGATCCACCATGGTTAATTTCCTGAGCGAAAACAG

(Continued on next page)

TABLE 1 (Continued)

Plasmids	Plasmid name	Cloning notes	Primer name	Primer sequence
		pCDNA3.1(+) OtDUB (1-675)-1xFlag was used as template. The primers contain 5′-BamHI and 3′-XhoI restriction sites, a 5′-start codon, and a 3′-1xFlag-stop codon. The amplicon was digested and ligated into like cut pCDNA3.1(+)		
			JMB681	GTACCTCGAGTTATTTATCGTCATCATCTTTGTAATCGCCTGAGC CAAATGGGATTGCTCTCAGAG
29	pCDNA3.1(+) OtDUB (170-675) V203D-1xFlag	pCDNA3.1(+) OtDUB (1-675) V203D-1xFlag was used as template. The primers contain 5′-BamHI and 3′-XhoI restriction sites, a 5′-start codon, and a 3′-1xFlag-stop codon. The amplic on was digested and ligated into like cut pCDNA3.1(+)	MZ276	GTACGGATCCACCATGGTTAATTTCCTGAGCGAAAACAG
			JMB681	GTACCTCGAGTTATTTATCGTCATCATCTTTGTAATCGCCT GAGCCAAATGGGATTGCTCTCAGAG
30	pCDNA3.1(+) OtDUB (675-1369)-1xFlag	Previously published in Lim et al. (15)		
31	pCDNA3.1(+) OtDUB (275-1369)-1xFlag	Previously published in Lim et al. (15)		
32	pCDNA3.1(+) OtDUB (275-675)-1xFlag	pCDNA3.1(+) OtDUB (1-1369)-1xFlag was used as template. The primers contain 5′-BamHI and 3′-XhoI restriction sites, a 5′-start codon, and a 3′-1xFlag-stop codon. The amplicon was dige sted and ligated into like cut pCDNA3.1(+)	JMB680	GTACGGATCCACCATGGCAAGCGCCGAAGTGTCTTCC
			JMB681	GTACCTCGAGTTATTTATCGTCATCATCTTTGTAATCGCCTG AGCCAAATGGGATTGCTCTCAGAG
33	pCDNA3.1(+) OtDUB (260-675)-1xFlag	pCDNA3.1(+) OtDUB (1–675)-1xFlag was used as template. The primers contain 5′-BamHI and 3′-XhoI restriction sites, a 5′-start codon, and a 3′-1xFlag-stop codon. The amplicon was diges ted and ligated into like cut pCDNA3.1(+)	MZ277	GTACGGATCCACCATGGAGAAGTTCAACAAATCCACTGC
			JMB681	GTACCTCGAGTTATTTATCGTCATCATCTTTGTAATCGCCTG AGCCAAATGGGATTGCTCTCAGAG
34	pCDNA3.1(+) OtDUB 675-1369-1xFlag E928K	Site-directed mutagenesis of pCDNA3.1(+) OtDUB (675-1369)-1xFlag to generate E928K	JMB821	GAGCTAAAATCCTGTACAAGGGCCCTGATGGAGTGG
			JMB822	GGATTTTAGCTCTGTCAAAATCTCTTTTGGATTGGG
35	pCDNA3.1(+) OtDUB 675-1369-1xFlag G997D	Site-directed mutagenesis of pCDNA3.1(+) OtDUB (675-1369)-1xFlag to generate G997D	JMB823	GAGGTGACAGATGCGATATTCTGATCGACGCTTCAAACGG
			JMB824	CATCTGTCACCTCCATCGAAAATCATACCGGTGCTATTGG
36	pCDNA3.1(+) OtDUB 675-1369-1xFlag L825P	Site-directed mutagenesis of pCDNA3.1(+) OtDUB (675-1369)-1xFlag to generate L825P	JMB817	CAGTTGCCGAGCGATTTGGCCAACCTGTCTAAGTTGC
			JMB818	CGCTCGGCAACTGTTTTGCGTGCTTGTTCTCC
37	pCDNA3.1(+) OtDUB 675-1369-1xFlag Q879R	Site-directed mutagenesis of pCDNA3.1(+) OtDUB (675-1369)-1xFlag to generate Q879R	JMB819	GTTGCGGCCCGCCAAATGCTCTGCCCAAGCTTTGCTG
			JMB820	CGGGCCGCAACATTGCATCAGGCAGCTCGGAACAC
38	pCDNA3.1(+) OtDUB 675-1369-1xFlag C1053Y	Site-directed mutagenesis of pCDNA3.1(+) OtDUB (675-1369)-1xFlag to generate C1053Y	JMB805	CAGGCTACTCAAGCGCCCCTCAAATTCTGATCAATATGCAC
			JMB806	GCTTGAGTAGCCTGGAATGAATTTGTCACCGGTCATGTTGGAAATGTCC
39	pCDNA3.1(+) OtDUB 675-1369-1xFlag G1052D	Site-directed mutagenesis of pCDNA3.1(+) OtDUB (675-1369)-1xFlag to generate G1052D	JMB807	CATTCCAGACTGCTCAAGCGCCCCTCAAATTCTGATCAATATGCAC
			JMB808	GAGCAGTCTGGAATGAATTTGTCACCGGTCATGTTGGAAATGTCC
40	pCDNA3.1(+) OtDUB 675-1369-1xFlag G969D	Site-directed mutagenesis of pCDNA3.1(+) OtDUB (675-1369)-1xFlag to generate G969D	JMB811	CAACAGGACAATTTCAGATCAGGAAGCACTGCCATCTATGGTG
			JMB812	CTGAAATTGTCCTGTTGCCAAGAGGTAACCAGAAATTCCTTCTGC
41	pCDNA3.1(+) OtDUB 675-1369-1xFlag K983N	Site-directed mutagenesis of pCDNA3.1(+) OtDUB (675-1369)-1xFlag to generate K983N	JMB803	GCTCAAACTTTTCTTCCAATAGCACCGGTATGATTTTCGATGG
			JMB804	GAAGAAAAGTTTGAGCCACCATAGATGGCAGTGCTTCCTGATCTG
42	pCDNA3.1(+) OtDUB 675-1369-1xFlag L824F	Site-directed mutagenesis of pCDNA3.1(+) OtDUB (675-1369)-1xFlag to generate L824F	JMB801	GCAAAACAGTTCCTGAGCGATTTGGCCAACCTGTCTAAGTTGC
			JMB802	CTCAGGAACTGTTTTGCGTGCTTGTTCTCCAATTCATTCAGC
43	pCDNA3.1(+) OtDUB 675-1369-1xFlag R972K	Site-directed mutagenesis of pCDNA3.1(+) OtDUB (675-1369)-1xFlag to generate R972K	JMB813	GCAATTTCAAATCAGGAAGCACTGCCATCTATGG TGGCTCAAAATTTTCTTCC
			JMB814	CCTGATTTGAAATTGCCCTGTTGCCAAGAGGTAACCAGAAATTCCTTCTGC
44	pCDNA3.1(+) OtDUB 675-1369-1xFlag S1054P	Site-directed mutagenesis of pCDNA3.1(+) OtDUB (675-1369)-1xFlag to generate S1054P	JMB809	CTGCCCAAGCGCCCCTCAAATTCTGATCAATATGCAC
			JMB810	CGCTTGGGCAGCCTGGAATGAATTTGTCACCGGTCATGTTGG
Yeast plasmids				
45	p416GAL OtDUB (1-1369)-1xFlag	Subcloned insert from pCDNA3.1(+) OtDUB (1-1369)-1xFlag using flanking-BamHI/XhoI sites		
46	p416GAL OtDUB (1-1369) C135A-1xFlag	Previously published in Lim et al. (15)		
47	p416GAL OtDUB (675–1369)-1xFlag	Previously published in Lim et al. (15)		
48	p416GAL OtDUB (275-1369)-1xFlag	Previously published in Lim et al. (15)		

(Continued on next page)

TABLE 1 (Continued)

Plasmids	Plasmid name	Cloning notes	Primer name	Primer sequence
49	p416GAL OtDUB (275-675)-1xFlag	Subcloned insert from pCDNA3.1(+) OtDUB (275-675)-1xFlag using flanking-BamHI/XhoI sites into like cut p416GAL1		
50	p416GAL1-OtDUB 3xFlag-6His 275-1186	Site-directed mutagenesis of p416GAL1 3xFlag-6His OtDUB 275-1369 1xFlag introducing a stop codon at 1187	JMB771	GAGCTTGATCTGGCGTGGATTCTTCCTCATTGCATG
			JMB772	CAGATCAAGCTCTTTTAACGATGTCCAGAATATCCTC
51	p416GAL1-OtDUB 3xFlag-6His 275-1234	Site-directed mutagenesis of p416GAL1 3xFlag-6His OtDUB 275-1369 1xFlag introducing a stop codon at 1235	JMB773	CTGAATAGCACGGCAATATCTACGATAAGGACGTG
			JMB774	CGTGCTATTCAGAAAAGAAAGTGTCCAAGCATTTACCG
52	p416GAL1 3xFlag-6His OtDUB 275-1062	Site-directed mutagenesis of p416GAL1 3xFlag-6His OtDUB 275-1369 1xFlag introducing a stop codon at 1063	JMB764	GATCAATTAGCACAAGTTCGATCCTGCCGTGTCTGTGCTGGAC
			JMB765	CTTGTGCTAATTGATCAGAATTTGAGGGGCGCTTGAGC
53	p416GAL1 3xFlag-6His OtDUB 275-1159	Site-directed mutagenesis of p416GAL1 3xFlag-6His OtDUB 275-1369 1xFlag introducing a stop codon at 1160	JMB766	CCGATAATAAGTAGTTGAAAACAGAACCCGACATCCAATCCAG
			JMB767	CTGTTTTCAACTACTTATTATCGGAGTTCTGAGAATAAAC
54	p416GAL1 3xFlag-6His OtDUB 275-1282	Site-directed mutagenesis of p416GAL1 3xFlag-6His OtDUB 275-1369 1xFlag introducing a stop codon at 1283	JMB768	CCAAGTAAAACAATAAGAAGGGTTGGCATGGCGCATGGG
			JMB769	CCTTCTTATTGTTTTACTTGGACACCAACTTTTTAACCATAGCAG
55	p416GAL1 3xFlag-6His OtDUB 275-1369 1xFlag	Subcloned insert from pCDNA3.1(+) OtDUB (275-1369)-1xFlag using flanking-BamHI/XhoI restriction sites and ligating into like cut p416GAL1 3xFlag-6His which contains an upstream, in-frame 3xFlag-6His tag		
56	p416GAL1 OtDUB 650-1369-1xFlag	pCDNA3.1(+) OtDUB (1-1369)-1xFlag was used as template. The primers contain 5′-BamHI and 3′-XhoI restriction sites and a 3′-1xFlag-stop codon. The amplicon was digested and ligated into like cu t p416GAL1	JMB829	GTACGGATCCACCATGAAGTTGTTCGATGACAACG
		JMB673		GTACCTCGAGCTATTTATCGTC
57	p416GAL1 OtDUB 760-1369-1xFlag	pCDNA3.1(+) OtDUB (1-1369)-1xFlag was used as template. The primers contain 5′-BamHI and 3′-XhoI restriction sites and a 3′-1xFlag-stop codon. The amplicon was digested and ligated into like cut p416GAL1	JMB728	GTACGGATCCACCATGTCTAGAGATGTGACTCTG
			JMB673	GTACCTCGAGCTATTTATCGTC
58	p416GAL1 OtDUB 797-1369-1xFlag	pCDNA3.1(+) OtDUB (1-1369)-1xFlag was used as template. The primers contain 5′-BamHI and 3′-XhoI restriction sites and a 3′-1xFlag-stop codon. The amplicon was digested and ligated into like cut p416GAL1	JMB729	GTACGGATCCACCATGGGATTGAAGGGTCTGTACG
			JMB673	GTACCTCGAGCTATTTATCGTC
59	p416GAL1 OtDUB 840-1369-1xFlag	pCDNA3.1(+) OtDUB (1-1369)-1xFlag was used as template. The primers contain 5′-BamHI and 3′-XhoI restriction sites and a 3′-1xFlag-stop codon. The amplicon was digested and ligated into like cut p416GAL1	JMB730	GTACGGATCCACCATGATCCTGCCAGAGTTTAAAGATG
			JMB673	GTACCTCGAGCTATTTATCGTC
60	p415GAL1 OtDUB-650-1159-URA3-HA	The pCDNA3.1(+) OtDUB (1-1369)-1xFlag was used as template to amplify codons 650-1159 with JMB779/780, which have a 5′-SpeI site, and a 3′-BamHI site, which was then ligated in like cut p415GAL1. The *S. cerevisiae* URA3 gene was amplified with JMB775/789 containing a 5′-BamHI site and a 3′-HA epitope and SalI site and ligated into-BamHI/SalI cut p415GAL1 OtDUB 650-1159 in-frame with the upstream codons	JMB775	GTACGGATCCGGTTCGAAAGCTACA TATAAGGAACGTG
			JMB789	GTACGTCGACTCACGCATAGTCAGGAACATCGTATGGGTATCCTGATCCG TTTTGCTGGCCGCATCTTCTC
			JMB779	GTACACTAGTACCATGAAGTTGTTCGATGACAACG
			JMB780	GTACGGATCCCTTATTATCGGAGTTCTGAG
61	p415GAL1 OtDUB-650-1186-URA3-HA	The above cloning strategy for p415GAL1 OtDUB-650-1159-URA3-HA was repeated with JMB780 replaced with JMB783 to amplify 650–1186	JMB779	GTACACTAGTACCATGAAGTTGTTCGATGACAACG
			JMB783	GTACGGATCCAGCTCTTTTAACGATGTCCAG
62	p415GAL1 OtDUB-650-1234-URA3-HA	The above cloning strategy for p415GAL1 OtDUB-650-1159-URA3-HA was repeated with JMB780 replaced with JMB782 to amplify 650–1234	JMB779	GTACACTAGTACCATGAAGTTGTTCGATGACAACG
			JMB782	GTACGGATCCTTCAGAAAAGAAAGTGTCCAAGC
63	p415GAL1 OtDUB-650-1282-URA3-HA	The above cloning strategy for p415GAL1 OtDUB-650-1159-URA3-HA was repeated with JMB780 replaced with JMB781 to amplify 650–1282	JMB779	GTACACTAGTACCATGAAGTTGTTCGATGACAACG
			JMB781	GTACGGATCCCTTGGACACCAACTTTTTAACC
64	p415GAL1 OtDUB-650-1282-URA3-HA A1069V	Site-directed mutagenesis of p415GAL1 OtDUB-650-1282-URA3-HA to generate A1069V	JMB815	GATCCTGTCGTGTCTGTGCTGGACATCCCCGAAGGCTTGAAAATTACCAG
			JMB816	GACACGACAGGATCGAACTTGTGCATATTGATCAGAATTTGAGG
65	p415GAL1 OtDUB-650-1282-URA3-HA C1053Y	Site-directed mutagenesis of p415GAL1 OtDUB-650-1282-URA3-HA to generate C1053Y	JMB805	CAGGCTACTCAAGCGCCCCTCAAATTCTGATCAATATGCAC
			JMB806	GCTTGAGTAGCCTGGAATGAATTTGTCACCGGTCATGTTGGAAATGTCC
66	p415GAL1 OtDUB-650-1282-URA3-HA G1052D	Site-directed mutagenesis of p415GAL1 OtDUB-650-1282-URA3-HA to generate G1052D	JMB807	CATTCCAGACTGCTCAAGCGCCCCTCAAATTCTGATCAATATGCAC
			JMB808	GAGCAGTCTGGAATGAATTTGTCACCGGTCATGTTGGAAATGTCC
67	p415GAL1 OtDUB-650-1282-URA3-HA G969D		JMB811	CAACAGGACAATTTCAGATCAGGAAGCACTGCCATCTATGGTG

(Continued on next page)

TABLE 1 (Continued)

Plasmids	Plasmid name	Cloning notes	Primer name	Primer sequence
		Site-directed mutagenesis of p415GAL1 OtDUB-650-1282-URA3-HA to generate G969D		
			JMB812	CTGAAATTGTCCTGTTGCCAAGAGGTAACCAGAAATTCCTTCTGC
68	p415GAL1 OtDUB-650-1282-URA3-HA K983N	Site-directed mutagenesis of p415GAL1 OtDUB-650-1282-URA3-HA to generate K983N	JMB803	GCTCAAACTTTTCTTCCAATAGCACCGGTATGATTTTCGATGG
			JMB804	GAAGAAAAGTTTGAGCCACCATAGATGGCAGTGCTTCCTGATCTG
69	p415GAL1 OtDUB-650-1282-URA3-HA L824F	Site-directed mutagenesis of p415GAL1 OtDUB-650-1282-URA3-HA to generate L824F	JMB801	GCAAAACAGTTCCTGAGCGATTTGGCCAACCTGTCTAAGTTGC
			JMB802	CTCAGGAACTGTTTTGCGTGCTTGTTCTCCAATTCATTCAGC
70	p415GAL1 OtDUB-650-1282-URA3-HA R972K	Site-directed mutagenesis of p415GAL1 OtDUB-650-1282-URA3-HA to generate R872K	JMB813	GCAATTTCAAATCAGGAAGCACTGCCATCTATGGTGGCTCAAAATTTTCTTCC
			JMB814	CCTGATTTGAAATTGCCCTGTTGCCAAGAGGTAACCAGAAATTCCTTCTGC
71	p415GAL1 OtDUB-650-1282-URA3-HA S1054P	Site-directed mutagenesis of p415GAL1 OtDUB-650-1282-URA3-HA to generate S1054P	JMB809	CTGCCCAAGCGCCCCTCAAATTCTGATCAATATGCAC
			JMB810	CGCTTGGGCAGCCTGGAATGAATTTGTCACCGGTCATGTTGG
72	p415GAL1 URA3-3HA-6His	URA3-3HA-6His was amplified from a previously published plasmid in Xie et al. (36) and inserted into p415MET25 using the flanking HindIII and XhoI sites. The insert was then excised and inserted into p415GAL1 using the same restriction sites	CMH329	GCATAAGCTTATGTCGAAAGCTACATATAAGG
			CMH330	GCATCTCGAGTCAGTGATGGTGGTGATGGTG
73	p416 GPD Lact-C2 GFP	Previously published in Yeung et al. (25)		

frozen in liquid N_2 and stored at −80°C. Protein concentration was determined by the bicinchoninic acid assay (23227; ThermoFisher).

AP-2 full-length and AP-2 μ2CTD-truncated cores were purified as previously described (35). Briefly, Rosetta DE3 cells were transformed with two Duet vectors: pETDuet encoding human β2(1–591) and human full-length μ2(1–435) or CTD-truncated(1–135); and pCDFDuet encoding rat α(1–621) with a C-terminal GST tag and human σ2(1–142). Transformed cells were grown at 37°C in the presence of 100 μg/mL each ampicillin and streptomycin, and protein expression was induced with 500 μM IPTG at 22°C for 16 h. Cell pellets were resuspended in lysis buffer and disrupted by several rounds of microfluidization before clarification by high-speed centrifugation. AP-2 cores were then affinity purified exactly as the AP-1 core.

For expression of μ2CTD alone, codons 159–435 of human μ2 were cloned into the pMAT9S vector, encoding an N-terminal maltose-binding protein (MBP) affinity tag as previously described (35). Expression of MBP-μ2CTD also required coexpression with the pGro7 vector, which encodes the GroEL/ES chaperone. Rosetta DE3 cells were transformed with both MBP-μ2CTD/pMAT9S and pGro7 and grown at 37°C in the presence of 100 μg/mL each ampicillin and chloramphenicol; chaperone expression was induced with 1.5 g/L L-(+)-arabinose at $A_{600} \sim 0.2$, and MBP-μ2CTD/expression was induced at $A_{600} \sim 0.8$ by 500 μM IPTG at 18°C for 16 h. Proteins were purified by Ni-NTA and amylose resin (E8021L; NEB), followed by overnight cleavage of the MBP tag by TEV protease (1:100 mass ratio) and dialysis into cation exchange buffer (25 mM HEPES pH 7, 50 mM NaCl, 0.1 mM TCEP). Isolated μ2CTD was further purified by cation exchange chromatography (HiTrap S) using a linear gradient from 0 to 1 M NaCl followed by size exclusion chromatography.

Recombinant OtDUB pulldowns of HeLa lysates. Frozen HeLa cell pellets were thawed on ice and resuspended in lysis buffer ± 20 mM NEM 50 mM Tris-HCl pH 7.5, 150 mM NaCl, 1% Triton X-100, 2 mM PMSF, and protease inhibitor tablet (cOmplete, 11697498001; Roche). After lysis, the insoluble fraction was pelleted, and clarified lysates were quantified by Bradford assay. Normalized lysates (4 mg/mL, 1-mL aliquots) were incubated with ~25 μg of OtDUB-C135A-Flag and rotated overnight at 4°C. Prewashed Flag M2 resin was added to each tube and rotated at 4°C for an additional hour. Pelleted resin was washed three times with 1 mL wash buffer (50 mM Tris-HCl pH 7.5, 150 mM NaCl, 0.1% Triton X-100) and then incubated for 15 min at 37°C in elution buffer (0.2 μg/mL 3xFlag peptide in wash buffer). Eluates were separated from the resin by transferring the sample to a Quick spin column (7326204; Bio-Rad) and centrifuged. Isolated eluates were quenched in SDS-PAGE sample-buffer and resolved alongside input lysates by SDS-PAGE.

Direct binding assays with OtDUB fragments and AP-1 or AP-2 core. Bacteria transformed with empty pGEX6P1 or various pGEX6P1-OtDUB fragments were grown overnight, back diluted in LB supplemented with 100 μg/mL of ampicillin and grown to an OD_{600} of 0.5–0.7, induced with 300 μM IPTG. After 16 h of growth at 18°C, ~40 mL of culture was pelleted and resuspended in 2 mL of 20 mM Tris-HCl pH 8.0, 200 mL NaCl, 1 mM DTT, 2 mM PMSF, and protease inhibitor tablet (cOmplete EDTA-free, 11873580001; Roche). Bacteria were then mechanically disrupted by sonication, and the insoluble fraction was removed by centrifugation. For each pulldown, 500 μL of clarified lysate was supplemented with 40 μL of prewashed glutathione resin slurry and 20 μg of purified AP-1 or AP-2 core. The samples were incubated with rotation for 1 h at 4°C and washed three times with 0.5 mL wash buffer (20 mM Tris-HCl pH 8.0, 200 mL NaCl, 1 mM DTT) before eluting in SDS-PAGE sample buffer and resolved by SDS-PAGE.

Size exclusion chromatography peak shift assays. For complex formation, $OtDUB_{C135A}$ (4 μM) or $OtDUB_{275–675}$ (22 μM) was incubated with either AP-1 core, AP-2 full core, μ2CTD-truncated AP-2 or AP-2 μ2CTD (2 μM with full-length and 11 μM with $OtDUB_{275–675}$) for 1 h at 37°C in 20 mM Tris-HCl pH 8.0, 200 mM NaCl, and 1 mM DTT in 600 μL total volume. After incubation, the sample was centrifuged for 5 min at 10,000 × *g*, and 500 μL was loaded onto a preequilibrated Superose 6 10/30 column and resolved at 4°C.

Cell culture and transfections. HeLa cells (ATCC) were cultured under standard conditions in complete medium (Dulbecco's modified Eagle's medium (DMEM) supplemented with 10% (vol/vol) antibiotic-free fetal bovine serum and 1% (vol/vol) penicillin/streptomycin). For transient transfections, cells were plated in 12-well plates containing coverslips (16004-300; VWR) (1×10^5 cells in 1 mL media) or in 10-cm plates (2.2×10^6 cells in 10 mL media); 24 h later, cells were transfected with the desired DNA using XtremeGENE9 (6365787001; Roche) according to the manufacturer's directions. In brief, 75 μL Opti-MEM, 3 μL XtremeGENE9, and 1 μg DNA for each milliliter of media were mixed and incubated at room temperature for 15 min before being adding dropwise to cells in antibiotic-free media.

Immunoprecipitations. HeLa cells ectopically expressing Flag-tagged OtDUB fragments for 24 h were collected by scraping in ice-cold PBS. The resulting cell pellet was then resuspended in lysis buffer (50 mM Tris-HCl pH 7.5, 150 mM NaCl, 0.2% Triton X-100, 2 mM PMSF, protease inhibitor tablet [cOmplete]). After thorough lysis on ice with intermittent vortexing the insoluble fraction was removed by pelleting, and the clarified lysate protein concentrations were determined by Bradford assay. Equal amounts of protein lysates were incubated with M2 Flag resin and rotated for 2 h at 4°C. Resin was then washed three times with 0.5 mL of wash buffer (lysis buffer without protease inhibitors) before being eluted in wash buffer + 0.4 μg/mL 3xFlag peptide and incubating for 15 min at 37°C. Samples were then loaded onto Quick spin columns to separate eluate from the resin. Eluates were mixed with SDS-PAGE sample buffer and resolved by SDS-PAGE alongside input lysates for downstream immunoblotting.

Fluorescent transferrin uptake assay. Twenty-four hours after transfection, HeLa cells plated on coverslips were washed twice in 37°C in serum-free (SF) DMEM medium and then incubated in SF medium for 60 min. The medium was then replaced with SF medium cooled to 4°C and containing 25 μg/mL of Alexa Fluor 568-labeled transferrin (T23365; ThermoFisher) and incubated for 15 min at 37°C before being processed for indirect immunofluorescence (below).

Indirect immunofluorescence. HeLa cells on coverslips were thoroughly washed with Tris-buffered saline (TBS) before each stage. Cells were first fixed in 3.7% formaldehyde in TBS for 15 min, permeabilized in 0.2% Triton X-100 in TBS for 15 min, and blocked in 3% (wt/vol) bovine serum albumin (BSA) in TBS for 1 h; all

steps were performed at room temperature. After blocking, coverslips were incubated with primary antibodies diluted in 3% BSA in TBS + 0.1% Triton X-100 for either 1 h at room temperature or overnight at 4°C in a humidified chamber. Coverslips were then incubated with Alexa Fluor-labeled secondary antibodies (Life Technologies) at 1:700 dilution for 1 h at room temperature in a humidified chamber before staining with Hoechst DNA stain (H3570; ThermoFisher) and mounting in Fluoromount-G (0100-01; Southern Biotech) on glass slides. Images were captured at ambient temperature with AxioVision (release 4.8.2.0) imaging software (Zeiss) controlling a Zeiss Axio Observer D1 microscope with a 63×/1.4 numerical aperture lens and an AxioCam MRm charge-coupled device camera (Zeiss).

Immunoblotting. Proteins resolved in SDS-PAGE gels were transferred to PVDF (Immobilon-P, IPVH00010; Millipore), and the membranes were blocked in either 5% (wt/vol) milk or 3% (wt/vol) BSA in TBS with 0.1% Tween 20 (TBST). After blocking, the membranes were incubated in primary antibody diluted in either milk or BSA depending on the antibody (see Antibodies section) for 1 h at room temperature or overnight at 4°C. Membranes were washed and then incubated with horseradish peroxidase (HRP)-conjugated secondary antibody (NA931V and NA934V; Cytiva) in the same blocking agent as the primary antibody for 1 h at room temperature, washed, and imaged by chemiluminescence (ECL) on a GBox (Syngene) imaging system or for Fig. 5C, autoradiography film (37).

Antibodies. Antibodies were used as follows: rabbit anti-ubiquitin (Dako, discontinued) at 1:2,000 for immunoblotting (membrane blocked with milk); mouse anti-AP1G1 (610385; BD Bioscience) at 1:5,00 for immunoblotting (BSA); mouse anti-AP2M1 (611350; BD Bioscience) at 1:500 for immunoblotting (BSA); mouse anti-Flag (F3165; Sigma) at 1:500 for immunofluorescence and 1:5,000 for immunoblotting (milk); mouse anti-HA (H9658; Sigma) at 1:5,000 for immunoblotting (milk); rabbit anti-OtDUB (YU1430 in-house antiserum) at 1:5,000-10,000 for immunoblotting (milk); rabbit anti-Rac1,2,3 (2465; Cell Signaling) at 1:1,000 for immunoblotting (BSA); rabbit anti-M6PR (PA3-850; ThermoFisher) at 1:100 for immunofluorescence; rabbit anti-GM130 (12480; Cell Signaling) at 1:3,200 for immunofluorescence; and rabbit anti-GST (ab111947; Abcam) at 1:5,000 for membrane lipid array analysis (BSA).

Yeast methods. *Saccharomyces cerevisiae* yeast were cultured under standard conditions at 30°C in either rich (yeast extract, peptone, and dextrose) or minimal medium (synthetic defined supplemented with nucleobases, amino acids, and dextrose) (38). The W303 background strain (39) (MHY2416) was used for all experiments except the *cho1*Δ analysis. For the latter, the BY4741 WT strain (MHY10139) was utilized along with the BY4741-derived *cho1*Δ*::kanMX4* deletion strain (clone ID 7756) obtained from Open Biosystems. In these experiments, choline and ethanolamine were each added to 1 mM (final). Plasmids were introduced by lithium acetate transformation (40), plated on selective media, and single colonies were isolated for use in ensuing experiments. For growth assays, transformants carrying the empty p416GAL1 vector (41) or p416GAL1-OtDUB variants were grown overnight in SD medium lacking uracil, and the cultures were diluted to an A_{600} of 0.2 OD units in 1 mL of sterile water. Samples were then serially diluted in 10-fold steps, and each dilution series was spotted onto minimal plates lacking uracil and either a noninducing (glucose) or inducing (galactose) carbon source. Plates were incubated at 30°C for 2 to 6 days before Gbox imaging.

To examine steady-state OtDUB protein levels, transformants were grown overnight in SD medium lacking uracil. The next day the cultures were back diluted into media lacking uracil and supplemented with 2% raffinose as a carbon source and grown overnight. On the last day, 2.5 OD units were diluted into medium lacking uracil with 2% galactose and grown for 4 h at 30°C after which 2.5 OD units were recovered, and the resulting yeast pellet was processed by alkaline treatment and SDS lysis (42) prior to immunoblot analysis.

Yeast selection for suppressors of OtDUB toxicity. The growth-based search for suppressors was carried out similarly to a previously published positive selection for mutants (43). Yeast were transformed with p415GAL1-based constructs encoding URA3-3HA, $OtDUB_{650–1159}$-URA3-HA, $OtDUB_{650–1234}$-URA3-HA, or $OtDUB_{650–1282}$-URA3-HA and plated on SD medium lacking leucine. The transformants were then evaluated on galactose-containing SD-LEU plates to verify toxicity. $OtDUB_{650–1159}$-URA3-HA was not toxic, unlike the longer constructs, and was used as a control in further experiments. The p415GAL1-$OtDUB_{650–1282}$-URA3-HA plasmid was digested with HindIII and BamHI to remove the toxic domain DNA. Separately, the same plasmid was used as template in high-fidelity polymerase chain reactions (Phusion, E0553L; NEB) to amplify DNA between codon 748 of the OtDUB sequence and the 5′ end of the *URA3* gene using primers JMB656/792. The ends of the PCR product therefore overlapped the sequences remaining in the gapped parent plasmid. Given the relatively large PCR fragment being screened (~1.6 kb), a high-fidelity polymerase was required to keep the frequency of mutations low enough to maximize the fraction of single-residue changes per fragment. When low-fidelity *Taq* polymerase-mediated PCR was used, most of the recovered transformants had greater than or equal to two codon changes (29 out of 31). The gapped plasmid and PCR amplicons were then gel purified (28706; Qiagen).

Gapped plasmid was transformed alone or along with different amounts of the PCR product into WT yeast. The cotransformations were expected to yield circular plasmids resulting from homologous recombination-based gap repair (Fig. 4C); the reconstituted circular plasmids are stable in cells and can be identified by growth on SD-LEU. Transformants were plated on SD-LEU plates and grown for 2 days at 30°C, then replica plated onto SD-URA+GAL plates. Colonies that grew within 2 to 3 days at 30°C were isolated by patching onto fresh SD-LEU plates, grown overnight in SD-LEU liquid media, and then processed for DNA extraction (38).

The resulting DNA was electroporated into DH5α *E. coli*, plated on LB-agar plates supplemented with ampicillin, and incubated overnight at 37°C to recover the plasmids. Bacterial transformants were then grown overnight in LB + ampicillin liquid cultures. The plasmids were isolated, and the DNA was sequenced, using primers JMB793, 656, and 657, across the entire region that had been PCR amplified. Of the 94 plasmids sequenced, 43 contained single-codon mutations, 37 had more than 1 codon mutated, 11 were gap repair failures, and 3 contained premature stop codons.

Yeast microscopy. The W303 strain (MHY2416) was cotransformed with either p415GAL1 vector or p415GAL1-OtDUB650-1369-Flag along with p416GPD-Lact-C2-GFP vector and plated on selective media. Transformants were grown overnight in SD medium lacking uracil and leucine, and the cultures were diluted into media lacking uracil and leucine with 2% raffinose and grown overnight. The next day, the cultures were diluted to an A_{600} of 0.2 OD units in medium lacking uracil and leucine and supplemented with 2% galactose and grown for 4 h at 30°C (OD_{600} of 0.5–0.6). Cells were collected by centrifugation (4,000 rpm, 3 min), washed with sterile water, and resuspended in fresh medium. Cells were mounted on glass slides and sealed under coverslips with nail polish. Yeast were visualized at ambient temperature on an Axioskop microsope (Zeiss) with a Plan-Apochromat 100×/1.40 oil DIC objective and an AxioCam MRm CCD camera (Zeiss). Epifluorescence images were captured using AxioVision software.

Protein-lipid overlay assay. Membrane strips each spotted with 15 different membrane lipids at 100 pmol per spot were obtained from Echelon Biosciences (P-6001, PIP Strip; P6002, Membrane Lipid Strip) and processed as suggested by the manufacturer. In brief, the membranes were first spotted with positive controls 1 μL secondary antibody, 100 ng $OtDUB_{C135A}$-Flag, or 500 pg of PI(4,5)P2 Grip (GST-PLC-d1-PH) from Echelon Biosciences (G-4501), blocked for 1 h in 3% BSA in TBST and then incubated for 1 h with 0.5–2 μg/mL of the indicated recombinant OtDUB polypeptides diluted in 3% BSA in TBST. Filters were then immunoblotted with anti-OtDUB or anti-GST antibodies and HRP-conjugated secondary antibodies as described in the immunoblotting section above.

Liposome sedimentation assay. The liposome sedimentation assay was carried out as previously described (44). Individual lipids obtained from Avanti Polar Lipids were resuspended in chloroform and included: DOPC (850375), DOPS (840035), cholesterol (700100), and PI_3P (850150). Liposomes were composed of 0% or 30% DOPS, 20% cholesterol, 1% PI_3P, and 79% or 49% DOPC by adding adjusted quantities to a glass round-bottom flask, evaporating the chloroform under a nitrogen gas stream, and resuspending the lipids in 400 μL of 50 mM Tris HCl pH 7.5, 150 mM NaCl to a final concentration of 2.5 mM and transferring to a microfuge tube. The suspensions were freeze-thaw cycled eight times by transferring between liquid nitrogen and a 37°C water bath. To generate liposomes of uniform size, the suspensions were then passed through a room temperature mini-extruder 21 times (610000; Avanti Polar Lipids Cat) loaded with either 0.2 (n = 1)- or 0.4-μm (n = 2) polycarbonate membranes (610006 and 610007; Avanti Polar Lipids). The resulting liposomes were transferred to a new microfuge tube and placed on ice. For each binding reaction, 20 μL of 2.5 mM liposomes was mixed with 1 μL of 80 μM protein to obtain a final protein concentration of 4 μM within a polycarbonate ultracentrifuge tube (343775; Beckman Coulter). The tube was covered with parafilm and incubated for 30 min at 37°C. Liposome:protein complexes were then pelleted at 100,000 × g for 20 min at 4°C in a TLA100 rotor in a benchtop ultracentrifuge. The supernatants were carefully removed, and the pellets were resuspended in SDS-PAGE sample buffer, resolved by SDS-PAGE, and stained for protein (GelCode Blue).

ACKNOWLEDGMENTS

We thank Jim Hurley for the AP1 plasmid, Christopher Burd for the Lact-C2-GFP plasmid, Pietro De Camilli for antibodies, Christian Schlieker for liposome reagents and equipment, and Shengyan Jin for help with one round of the yeast mutagenesis screen and for testing domains needed for minimal OtDUB toxicity in yeast. We also thank Carolyn Machamer for expert advice and comments on the manuscript.

This work was supported by NIH grant GM136325 (to M.H.).

REFERENCES

1. Watt G, Parola P. 2003. Scrub typhus and tropical rickettsioses. Curr Opin Infect Dis 16:429–436. https://doi.org/10.1097/00001432-200310000-00009.
2. Xu G, Walker DH, Jupiter D, Melby PC, Arcari CM. 2017. A review of the global epidemiology of scrub typhus. PLoS Negl Trop Dis 11:e0006062. https://doi.org/10.1371/journal.pntd.0006062.
3. Diaz FE, Abarca K, Kalergis AM. 2018. An update on host-pathogen interplay and modulation of immune responses during Orientia tsutsugamushi infection. Clin Microbiol Rev 31:e00076-17. https://doi.org/10.1128/CMR.00076-17.
4. Chu H, Lee JH, Han SH, Kim SY, Cho NH, Kim IS, Choi MS. 2006. Exploitation of the endocytic pathway by Orientia tsutsugamushi in nonprofessional phagocytes. Infect Immun 74:4246–4253. https://doi.org/10.1128/IAI.01620-05.
5. Evans SM, Rodino KG, Adcox HE, Carlyon JA. 2018. Orientia tsutsugamushi uses two Ank effectors to modulate NF-kappaB p65 nuclear transport and inhibit NF-kappaB transcriptional activation. PLoS Pathog 14:e1007023. https://doi.org/10.1371/journal.ppat.1007023.
6. Beyer AR, Rodino KG, VieBrock L, Green RS, Tegels BK, Oliver LD, Jr, Marconi RT, Carlyon JA. 2017. Orientia tsutsugamushi Ank9 is a multifunctional effector that utilizes a novel GRIP-like Golgi localization domain for Golgi-to-endoplasmic reticulum trafficking and interacts with host COPB2. Cell Microbiol 19:e12727. https://doi.org/10.1111/cmi.12727.
7. Beyer AR, VieBrock L, Rodino KG, Miller DP, Tegels BK, Marconi RT, Carlyon JA. 2015. Orientia tsutsugamushi strain Ikeda ankyrin repeat-containing proteins recruit SCF1 ubiquitin ligase machinery via poxvirus-like F-box motifs. J Bacteriol 197:3097–3109. https://doi.org/10.1128/JB.00276-15.
8. VieBrock L, Evans SM, Beyer AR, Larson CL, Beare PA, Ge H, Singh S, Rodino KG, Heinzen RA, Richards AL, Carlyon JA. 2014. Orientia tsutsugamushi ankyrin repeat-containing protein family members are Type 1 secretion system substrates that traffic to the host cell endoplasmic reticulum. Front Cell Infect Microbiol 4:186. https://doi.org/10.3389/fcimb.2014.00186.
9. Rodino KG, VieBrock L, Evans SM, Ge H, Richards AL, Carlyon JA. 2018. Orientia tsutsugamushi modulates endoplasmic reticulum-associated degradation to benefit its growth. Infect Immun 86:e00596-17. https://doi.org/10.1128/IAI.00596-17.
10. Rodino KG, Adcox HE, Martin RK, Patel V, Conrad DH, Carlyon JA. 2019. The obligate intracellular bacterium Orientia tsutsugamushi targets NLRC5 to modulate the major histocompatibility complex class I pathway. Infect Immun 87:e00876-18. https://doi.org/10.1128/IAI.00876-18.
11. Adcox HE, Hatke AL, Andersen SE, Gupta S, Otto NB, Weber MM, Marconi RT, Carlyon JA. 2021. Orientia tsutsugamushi nucleomodulin Ank13 exploits the RaDAR nuclear import pathway to modulate host cell transcription. mBio 12:e0181621. https://doi.org/10.1128/mBio.01816-21.
12. Berk JM, Lim C, Ronau JA, Chaudhuri A, Chen H, Beckmann JF, Loria JP, Xiong Y, Hochstrasser M. 2020. A deubiquitylase with an unusually high-affinity ubiquitin-binding domain from the scrub typhus pathogen Orientia tsutsugamushi. Nat Commun 11:2343. https://doi.org/10.1038/s41467-020-15985-4.

13. Li SJ, Hochstrasser M. 1999. A new protease required for cell-cycle progression in yeast. Nature 398:246–251. https://doi.org/10.1038/18457.
14. Pruneda JN, Durkin CH, Geurink PP, Ovaa H, Santhanam B, Holden DW, Komander D. 2016. The molecular basis for ubiquitin and ubiquitin-like specificities in bacterial effector proteases. Mol Cell 63:261–276. https://doi.org/10.1016/j.molcel.2016.06.015.
15. Lim C, Berk JM, Blaise A, Bircher J, Koleske AJ, Hochstrasser M, Xiong Y. 2020. Crystal structure of a guanine nucleotide exchange factor encoded by the scrub typhus pathogen Orientia tsutsugamushi. Proc Natl Acad Sci U S A 117:30380–30390. https://doi.org/10.1073/pnas.2018163117.
16. Park SY, Guo X. 2014. Adaptor protein complexes and intracellular transport. Biosci Rep 34:e00123. https://doi.org/10.1042/BSR20140069.
17. Traub LM, Bonifacino JS. 2013. Cargo recognition in clathrin-mediated endocytosis. Cold Spring Harb Perspect Biol 5:a016790. https://doi.org/10.1101/cshperspect.a016790.
18. Ohno H, Stewart J, Fournier MC, Bosshart H, Rhee I, Miyatake S, Saito T, Gallusser A, Kirchhausen T, Bonifacino JS. 1995. Interaction of tyrosine-based sorting signals with clathrin-associated proteins. Science 269:1872–1875. https://doi.org/10.1126/science.7569928.
19. Kelly BT, McCoy AJ, Spate K, Miller SE, Evans PR, Honing S, Owen DJ. 2008. A structural explanation for the binding of endocytic dileucine motifs by the AP2 complex. Nature 456:976–979. https://doi.org/10.1038/nature07422.
20. Chen C, Nguyen BN, Mitchell G, Margolis SR, Ma D, Portnoy DA. 2018. The Listeriolysin O PEST-like sequence co-opts AP-2-mediated endocytosis to prevent plasma membrane damage during Listeria infection. Cell Host Microbe 23:786–795.e785. https://doi.org/10.1016/j.chom.2018.05.006.
21. Morrow ME, Morgan MT, Clerici M, Growkova K, Yan M, Komander D, Sixma TK, Simicek M, Wolberger C. 2018. Active site alanine mutations convert deubiquitinases into high-affinity ubiquitin-binding proteins. EMBO Rep 19:e45680. https://doi.org/10.15252/embr.201745680.
22. Doray B, Ghosh P, Griffith J, Geuze HJ, Kornfeld S. 2002. Cooperation of GGAs and AP-1 in packaging MPRs at the trans-Golgi network. Science 297:1700–1703. https://doi.org/10.1126/science.1075327.
23. Bos JL, Rehmann H, Wittinghofer A. 2007. GEFs and GAPs: critical elements in the control of small G proteins. Cell 129:865–877. https://doi.org/10.1016/j.cell.2007.05.018.
24. Atkinson KD, Jensen B, Kolat AI, Storm EM, Henry SA, Fogel S. 1980. Yeast mutants auxotrophic for choline or ethanolamine. J Bacteriol 141:558–564. https://doi.org/10.1128/jb.141.2.558-564.1980.
25. Yeung T, Gilbert GE, Shi J, Silvius J, Kapus A, Grinstein S. 2008. Membrane phosphatidylserine regulates surface charge and protein localization. Science 319:210–213. https://doi.org/10.1126/science.1152066.
26. Haglund K, Di Fiore PP, Dikic I. 2003. Distinct monoubiquitin signals in receptor endocytosis. Trends Biochem Sci 28:598–603. https://doi.org/10.1016/j.tibs.2003.09.005.
27. Andersen MH, Graversen H, Fedosov SN, Petersen TE, Rasmussen JT. 2000. Functional analyses of two cellular binding domains of bovine lactadherin. Biochemistry 39:6200–6206. https://doi.org/10.1021/bi992221r.
28. Uchida Y, Hasegawa J, Chinnapen D, Inoue T, Okazaki S, Kato R, Wakatsuki S, Misaki R, Koike M, Uchiyama Y, Iemura S, Natsume T, Kuwahara R, Nakagawa T, Nishikawa K, Mukai K, Miyoshi E, Taniguchi N, Sheff D, Lencer WI, Taguchi T, Arai H. 2011. Intracellular phosphatidylserine is essential for retrograde membrane traffic through endosomes. Proc Natl Acad Sci U S A 108:15846–15851. https://doi.org/10.1073/pnas.1109101108.
29. Kay JG, Fairn GD. 2019. Distribution, dynamics and functional roles of phosphatidylserine within the cell. Cell Commun Signal 17:126. https://doi.org/10.1186/s12964-019-0438-z.
30. Jackson LP, Kelly BT, McCoy AJ, Gaffry T, James LC, Collins BM, Honing S, Evans PR, Owen DJ. 2010. A large-scale conformational change couples membrane recruitment to cargo binding in the AP2 clathrin adaptor complex. Cell 141:1220–1229. https://doi.org/10.1016/j.cell.2010.05.006.
31. Di Paolo G, De Camilli P. 2006. Phosphoinositides in cell regulation and membrane dynamics. Nature 443:651–657. https://doi.org/10.1038/nature05185.
32. Ren X, Farias GG, Canagarajah BJ, Bonifacino JS, Hurley JH. 2013. Structural basis for recruitment and activation of the AP-1 clathrin adaptor complex by Arf1. Cell 152:755–767. https://doi.org/10.1016/j.cell.2012.12.042.
33. Fadok VA, Bratton DL, Frasch SC, Warner ML, Henson PM. 1998. The role of phosphatidylserine in recognition of apoptotic cells by phagocytes. Cell Death Differ 5:551–562. https://doi.org/10.1038/sj.cdd.4400404.
34. Murata-Kamiya N, Kikuchi K, Hayashi T, Higashi H, Hatakeyama M. 2010. Helicobacter pylori exploits host membrane phosphatidylserine for delivery, localization, and pathophysiological action of the CagA oncoprotein. Cell Host Microbe 7:399–411. https://doi.org/10.1016/j.chom.2010.04.005.
35. Kwon Y, Kaake RM, Echeverria I, Suarez M, Karimian Shamsabadi M, Stoneham C, Ramirez PW, Kress J, Singh R, Sali A, Krogan N, Guatelli J, Jia X. 2020. Structural basis of CD4 downregulation by HIV-1 Nef. Nat Struct Mol Biol 27:822–828. https://doi.org/10.1038/s41594-020-0463-z.
36. Xie Y, Rubenstein EM, Matt T, Hochstrasser M. 2010. SUMO-independent in vivo activity of a SUMO-targeted ubiquitin ligase toward a short-lived transcription factor. Genes Dev 24:893–903. https://doi.org/10.1101/gad.1906510.
37. Mruk DD, Cheng CY. 2011. Enhanced chemiluminescence (ECL) for routine immunoblotting: An inexpensive alternative to commercially available kits. Spermatogenesis 1:121–122. https://doi.org/10.4161/spmg.1.2.16606.
38. Guthrie C, Fink GR. 1991. Guide to yeast genetics and molecular biology: methods in enzymology, vol 194. Academic Press, San Diego, CA.
39. Thomas BJ, Rothstein R. 1989. Elevated recombination rates in transcriptionally active DNA. Cell 56:619–630. https://doi.org/10.1016/0092-8674(89)90584-9.
40. Gietz RD, Woods RA. 2002. Transformation of yeast by lithium acetate/single-stranded carrier DNA/polyethylene glycol method. Methods Enzymol 350:87–96. https://doi.org/10.1016/S0076-6879(02)50957-5.
41. Mumberg D, Muller R, Funk M. 1994. Regulatable promoters of Saccharomyces cerevisiae: comparison of transcriptional activity and their use for heterologous expression. Nucleic Acids Res 22:5767–5768. https://doi.org/10.1093/nar/22.25.5767.
42. Kushnirov VV. 2000. Rapid and reliable protein extraction from yeast. Yeast 16:857–860. https://doi.org/10.1002/1097-0061(20000630)16:9%3C857::AID-YEA561%3E3.0.CO;2-B.
43. Hickey CM, Xie Y, Hochstrasser M. 2018. DNA binding by the MATalpha2 transcription factor controls its access to alternative ubiquitin-modification pathways. Mol Biol Cell 29:542–556. https://doi.org/10.1091/mbc.E17-10-0589.
44. Ma M, Kumar S, Purushothaman L, Babst M, Ungermann C, Chi RJ, Burd CG. 2018. Lipid trafficking by yeast Snx4 family SNX-BAR proteins promotes autophagy and vacuole membrane fusion. Mol Biol Cell 29:2190–2200. https://doi.org/10.1091/mbc.E17-12-0743.